CHALMERS
UNIVERSITY OF TECHNOLOGY

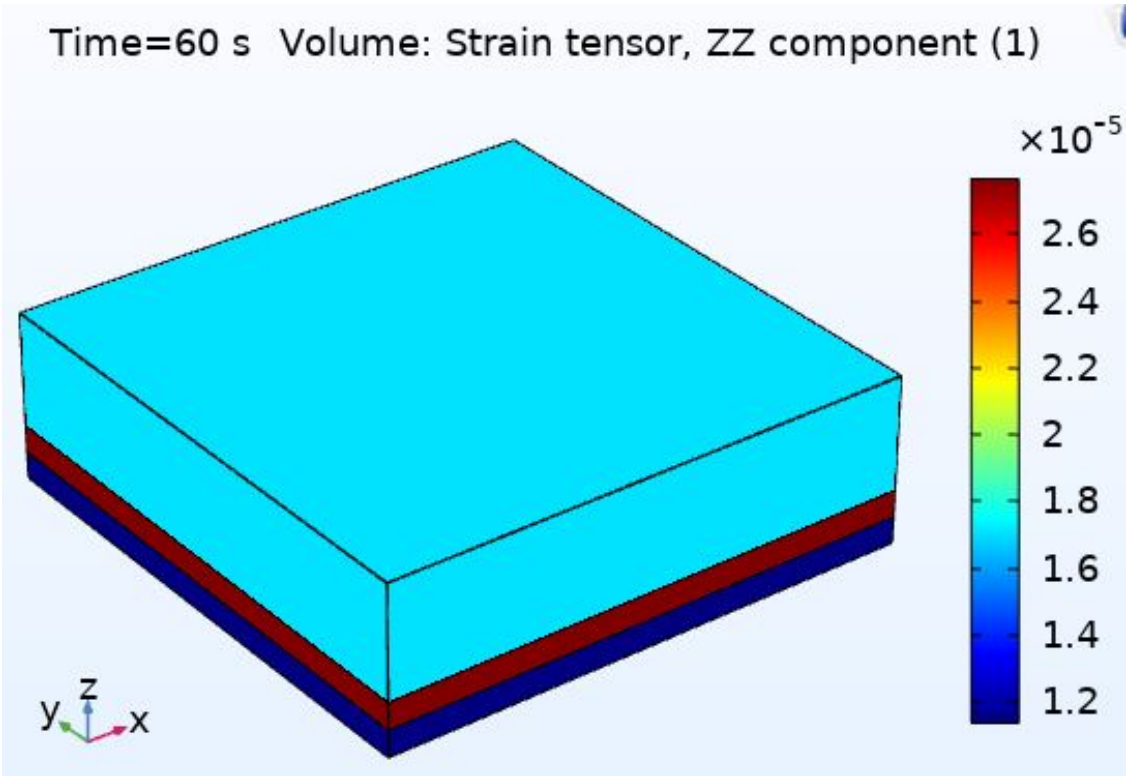

Thermo-mechanical modelling of structural battery composites

Master's thesis in Applied mechanics

Natasha Svensson

Department of Industrial and Materials science
CHALMERS UNIVERSITY OF TECHNOLOGY
Gothenburg, Sweden 2020

Master's thesis 2020:NN

Thermo-mechanical modelling of structural battery composites

Natasha Svensson

CHALMERS
UNIVERSITY OF TECHNOLOGY

Department of Industrial and Materials Science
Division of Material and Computational Mechanics
Chalmers University of Technology
Gothenburg, Sweden 2020

Thermo-mechanical modelling of structural battery composites
Natasha Svensson

Supervisor: David Carlstedt, Department of Industrial and Materials Science
Examiner: Leif Asp, Department of Industrial and Materials Science

Master's Thesis 2020:NN
Department of Industrial and Materials Science
Division of Material and Computational Materials
Chalmers University of Technology
SE-412 96 Gothenburg
Telephone +46 31 772 1000

Cover: Modelling made in COMSOL depicting the strain distribution in a structural battery composite cell at time 60 seconds, applied heat source 500 kW/m^3 and heat transfer coefficient 5 W/m^{2}K.

Typeset in LaTeX
Printed by Chalmers Reproservice
Gothenburg, Sweden 2020

Thermo-mechanical modelling of structural battery composites
Master Thesis
Natasha Svensson
Department of Industrial and Materials Science
Chalmers University of Technology

Abstract

Industries are searching for energy efficient zero-emission transport solutions to minimise environmental impact from transportation [1]. A possible solution to this can be the use of structural battery composites which combines the ability to take mechanical load while also store electrical energy [1], i.e. combining the functionalities of structures and batteries. The aim of this thesis is to develop a model which can predict the thermo-mechanical behaviour of a laminated structural battery composite. It is conducted in collaboration with an other master's thesis which instead focus on the battery modelling [2].

The laminated structural battery composite studied in this project has a similar structure to a regular Li-ion battery. The simplified model, made in COMSOL, was constructed as a three-layered battery unit cell where each layer's properties was approximated by using composite micro-mechanics models. The boundary conditions were such that only the top boundary was allowed to move while having a convective heat flux applied.

As the behaviour is only modelled (numerical investigation), i.e. no manufacturing or testing was conducted on real batteries, there is no way to know how good the modelled prediction actually compares to the reality. Instead investigation is made as a sensitivity study, to see how different parameters change the outcome which includes time, generated heat in the battery cell, heat transfer coefficient of the heat flux and thicknesses of the different layers.

The results show that after some time a steady state temperature will be reached as long as the heat transfer coefficient is non-zero. This steady state temperature is important for future thermal experiments as a too low temperature will give misleading results. This thesis has though shown that it can be controlled by changing e.g. the generated heat from the battery cell by changing the C-rate or the heat exchange with the surroundings. The conclusion is therefore that this developed framework, in combination with the collaborated thesis [2], can be used to guide future experiments on the thermo-mechanical behaviour of a laminated structural battery composite.

Keywords: Structural battery composite, COMSOL, Finite Element, composite mechanics, coupling, thermal-mechanical behaviour

Acknowledgements

This thesis was conducted at Chalmers University of Technology under the umbrella of the TRACKS-course called "TRA-105 Structural batteries – design, manufacture and characterisation". This course did not work out the way it was planned because of the Covid-19 pandemic which also directly affected the work on this thesis. Even through the pandemic, a thesis could be conducted and therefore I would like to show my deepest gratitude to those who helped me make this thesis possible:

My supervisor David Carlstedt (PhD Student at the division of Material and Computational Mechanics, Department of Industrial and Materials Science) for his guidance and feedback through out the whole project especially considering the extraordinary circumstances because of the Covid-19 pandemic.

My examiner Leif Asp (Professor at the division of Material and Computational Mechanics, Department of Industrial and Materials Science) for the feedback on my work and for helping me deliver this thesis on time.

My collaboration partner Mengyu Dong for sharing important results and problems with me from a electrochemical point-of-view.

I would also like to give my thanks to the other participants and teachers in the TRACKS-course for giving smaller feedback on my work under bi-weekly meetings and for giving better understanding in other fields of science than the one I am most familiar with e.g., electrochemistry.

Natasha Svensson, Gothenburg, June 2020

Contents

Nomenclature

Abbreviations

Al	Aluminium
FE	Finite Element
FEM	Finite Element Method
LFP	Lithium iron phosphate
Li	Lithium
NMC	Lithium-manganese-cobalt-oxide
PDE	Partial differential equations
PE	Polyethylene
PET	Polyethylene terephthalate
SBE	Structural battery electrolyte
SOC	State of charge

Indices

f	Fibre parameter
L	Longitudinal parameter
m	Matrix parameter
T	Transverse parameter
x, xy	In-plane parameter
z, xz	Out-of-plane parameter

List of symbols

α	Thermal expansion coefficient	[1/K]
β	Coefficient for hygroscopic-like electrochemical expansion.	
$\boldsymbol{\sigma}$	Stressvector	[-]
$\boldsymbol{b}$	Body forces	[N]
$\boldsymbol{q}$	Heat exchange	[W/m^2]
γ_{LT}	Shear strain	[-]
$\hat{C}$	Normalised lithium concentration	[-]
ν_{LT}	Major Poisson's ratio	[-]

ν_{TL}	Minor Poisson's ratio	[-]
ρ	Density	[kg/m^3]
τ_{LT}	Shear stress	[GPa]
ε^T	Thermal strain	[-]
ξ	Measure of reinforcement	[-]
a_i	Unknown variables	
C	Lithium Concentration	[mol/m^3]
C_p	Specific heat capacity	[J/(kgK)]
C_{sat}	Saturated lithium concentration	[mol/m^3]
E	Elastic modulus	[GPa]
G	Shear modulus	[GPa]
h	Heat transfer coefficient	[W/(m^{2}K)]
k	Thermal conductivity	[W/(mK)]
l	Length	[m]
n	Number of nodes	[-]
N_i	Basis functions	[-]
Q_{gen}	Generated heat	[W/m^3]
T	Temperature	[K]
t	Thickness	[m]
T_{ext}	External temperature	[K]
t_T	Time	[s]
V	Volume fraction	[-]
w	Width	[m]

List of Figures

List of Tables

1
Introduction

This chapter introduces the topic of this thesis through a background description together with related aim, milestones and limitations.

1.1 Background

As of present day, industries are searching for alternative ways to minimise the environmental impact, which usually comes from the usage of fossil fuel sources, but also to minimise the weight against power ratio [1]. The major problem with making, for example, an airplane fully electrical is the weight. To have the same amount of electrical energy as jet fuel, the weight of the aircraft would be too high, and take up much of its volume [3].

A possible solution to this problem can be to take advantage of a multi-functional material; in this case a structural battery composite. This type of materials can take mechanical load while also store electrical energy [1]. In other words, the material combines the functions of a battery with those of a mechanically strong composite material. Weight savings can be realised as the power source is incorporated with the body of e.g. the airplane instead of having two different components [3, 4]. Using rechargeable battery cells, can also lead to a smaller environmental impact if the energy comes from renewable energy sources.

The concept of structural batteries is relatively new and therefore much knowledge is still lacking. Hence, structural batteries can still not be introduced in industrial products. This is why this thesis is of importance providing new and necessary information about the concept, and further helps the development.

One of the biggest challenges in structural battery composites, as of now, is how the mechanical properties of the materials are affected by temperature changes inside the cell. Heat will be generated inside the structural battery composite due to the electrochemical processes which enables electrical energy storage. This generated heat will lead to shrinkage/expansion of the constituents in the material, which in turn will generate internal stresses [5, 6]. If these stresses become too high, there may be mechanical failure, which is one reason why the prediction of temperature distribution is of importance. The generated heat may also significantly affect the elastic properties of the polymer material of the structural battery electrolyte matrix, and consequently influence the stiffness of the structural battery [5, 6].

The focus of this thesis is on the thermo-mechanical behaviour of a structural battery composite, which includes studies on temperature, stress and strain distribution due to generated heat from electrochemical processes. Due to the Covid-19 pandemic, the study is limited to a numerical investigation, and no structural battery cells are manufactured and tested in the project.

1.2 Aim and milestones

The aim of this project is to develop a computational framework which can show the thermo-mechanical behaviour of a structural battery composite cell. The model will be made in the FE-software COMSOL and be modelled according to a laminated battery composite structure. The methods used are limited to calculations and computational modelling, i.e. no real physical battery cells will be constructed.

This thesis will be conducted in parallel and, to some degree, in collaboration with another master's thesis project conducted by Mengyu Dong with the title "Thermal Analysis and Battery Modelling for Structural Battery Composites" [2] which focus on the battery modelling from a electrochemical perspective.

1.2.1 Milestones

The project is divided into smaller milestones or objectives, which are presented below.

1.2.1.1 Material parameters

Material parameters for the structural battery composite cell will be approximated and calculated according to composite mechanics. These are needed as each layer in the battery composite cell will be some type of composite material.

1.2.1.2 Modelling

Modelling will be conducted of the laminated battery composite cell from a thermo-mechanical perspective.

1.2.1.3 Coupling

Coupling between the two models depicting the different behaviours of a structural battery composite i.e, thermo-mechanical (this thesis) and electrochemical (the collaborated thesis) will be conducted.

1.3 Limitations

The limitations of this thesis project are listed below in no specific order.

- Only structural batteries of type lithium-ion will be modelled. There will be no tests regarding different materials related to the battery cell
- Only the laminated type of structural battery composite will be modelled in this project i.e. no other types will be addressed
- The focus will be on the thermo-mechanical behaviour of structural batteries, which means that the aspect of the electrochemical processes, linked to the battery's functionality, will be kept to a minimum
- The battery will only be modelled in the scope of this project. There will be no manufacturing or testing conducted on a real physical battery cell [1]
- The commercial FE-software COMSOL will be used for modelling
- The FE-model will be developed for the composite part of a structural battery. The heat from the electrochemical processes will be calculated by another master's student and the results will be used as input data to the thermo-mechanical FE-model

[1] This was a direct consequence of the covid-19 pandemic.

2
Theory

This chapter explains the theoretical framework used in the scope of this thesis. The chapter is divided into four main sections; composite materials, battery, structural battery composite and the computational framework. Together these sections provide all essential information regarding structural battery composite cells.

2.1 Composite materials

The general definition of a composite is; a material made of two or more constituent materials that have different physical properties and chemically interfaces [7]. These constituents are divided into reinforcement (e.g. fibres or particles) and matrix, where reinforcement is the discontinuous phase and matrix is the continuous phase [7]. The constituents can also include a chemical sizing (coating of sorts) between the reinforcement and matrix to protect the reinforcement and to improve the interface strength between the fibre and the matrix. One commonly used composite material is carbon fibre reinforced polymer composites which is also the focus of this thesis as previous studies [1] have shown that this material is a viable candidate for structural battery application.

The properties of composite materials are determined by several different aspects, e.g. the choice of reinforcement and matrix, and the ratio between them (i.e. the volume fraction), etc. In the case of structural battery composites, the properties should be beneficial from both mechanical and electrochemical aspects.

2.1.1 Definitions

In this thesis composite related terms, which may or may not be clear for someone that has not studied or researched in the area, are used. Therefore, brief descriptions of terms used in this report are presented in this section.

2.1.1.1 Lamina and laminate

A lamina or ply is one layer of composite material while a laminate is a stack of these plies. A laminate can have different layups, i.e. how the different layers are stacked. These are dependent on the direction of the plies, with respect to the fibre orientation of the unidirectional lamina. A symmetric laminate is a laminate which is mirrored at the midplane [7]. A symmetric laminate will not warp due to swelling or shrinkage of the constituents (e.g. linked to temperature changes) as there is no

bending-extension coupling [7].

2.1.1.2 Perfect adhesion

Perfect adhesion means that the adhesion between two layers is infinitely small and cannot bend in shear. Therefore there is no slippage between the layers and there is continuous displacement throughout the adhesion layer [7].

2.1.1.3 Unidirectional lamina

Unidirectional lamina composite is transversely isotropic, i.e. isotropic in the yz-plane (Figure 2.1). For a unidirectional composite lamina, there are two directions which the properties can be defined in: longitudinal (index L) and transverse (index T). Longitudinal is the direction parallel to the fibres and the transverse is the direction perpendicular to the fibres. These are shown in Figure 2.1 below. The longitudinal properties of a lamina are often controlled by the fibres while the transverse properties are controlled by the matrix. [7]

Figure 2.1: The coordinates in an lamina with respect to the fibre where z-direction points outwards from the lamina.

For a material which has the same coordinate system as the Cartesian, i.e. the x-direction is parallel to the longitudinal direction, the material parameters are the same. Consequently, there is no need to transform stresses and strain in the ply. In contrast, for any other fibre orientation (e.g. for 45 degree plies) stresses and strains must be transformed to the L-T coordinate system.

2.1.1.4 Thermosets vs thermoplastics

In the case of fibre reinforced polymer composites, the matrix can be made from either thermosets or thermoplastics. These are defined by how they behave when a heat source is applied and how their microstructures are arranged [7]. Thermoplastics are polymers that will reshape or melt when heat is applied, this means that they can be reshaped if necessary as the process can be reversed. Thermosets, on the other hand, do not melt, instead they decompose when heat is applied. This process cannot be reversed, once too much heat is applied the material will degrade [7].

2.1.2 Mechanical properties

The mechanical properties of a lamina can be calculated by micro-mechanics models, according to e.g. rule of mixtures and Halpin-Tsai. In this section expressions for the elastic moduli (E), shear modulus (G) and Poisson's ratio (ν) are presented.

2.1.2.1 Elastic modulus

The longitudinal elastic modulus can be defined in accordance with the rule of mixtures as:

$$E_L = V_f E_f + V_m E_m \tag{2.1}$$

where indices f, m defines fibre or matrix, respectively. V is the volume fraction and E the elastic modulus. The volume fraction is often described for the fibre and the volume fraction of the matrix can easily be calculated as $V_m = 1 - V_f$.

The Halpin-Tsai model for transverse elastic modulus is defined as:

$$E_T = \frac{1 + \xi\eta V_f}{1 - \eta V_f} E_m \tag{2.2}$$

$$\eta = \frac{\frac{E_f}{E_m} - 1}{\frac{E_f}{E_m} + \xi} \tag{2.3}$$

where ξ is a measure of reinforcement. For circular fibres, this value is $\xi = 2$ [7].

Moreover, for particle-reinforced materials, the Nielsen model [8] is used when calculating the elastic moduli. The Nielsen model [8] is defined as:

$$E_c = E_m \left(\frac{1 + A\eta_N V_f}{1 - \psi\eta_N V_f} \right) \tag{2.4}$$

where $A = 1.5$ for spherical particles and η_N is defined as:

$$\eta_N = \frac{\frac{E_f}{E_m} - 1}{\frac{E_f}{E_m} + A} \tag{2.5}$$

and ψ is defined as:

$$\psi = 1 + \left(\frac{1 - \phi_{max}}{\phi_{max}^2} \right) \tag{2.6}$$

where $\phi_{max} = 0.7405$ for spherical particles.

Furthermore, the inverse rule of mixtures will also be used to calculate the transverse elastic modulus for the pouch-bag material. The inverse rule of mixtures for transverse elastic modulus is defined as:

$$E_T = \left(\frac{V_f}{E_f} + \frac{V_m}{E_m} \right)^{-1} \tag{2.7}$$

2.1.2.2 Shear modulus

The Halpin-Tsai model (Equations 2.2-2.3) can also be used to calculate the in-plane shear modulus (G_{LT}) for fibre-reinforced materials by changing from elastic moduli for the fibre and matrix to the shear moduli of these and changing the reinforcement ξ. Hence, the in-plane shear modulus is expressed as:

$$G_{LT} = \frac{1 + \xi\eta V_f}{1 - \eta V_f} G_m \tag{2.8}$$

$$\eta = \frac{\frac{G_f}{G_m} - 1}{\frac{G_f}{G_m} + \xi} \tag{2.9}$$

where G_f and G_m are the shear modulus for the fibre and matrix, respectively and $\xi = 1$.

For a orthotropic material with one plane of symmetry in the yz-plane, the shear modulus in the isotropic plane can be calculated as:

$$G_{TT} = \frac{E_T}{2(1 + \nu_{LT})} \tag{2.10}$$

where ν_{LT} is the major Poisson's ratio which is explained later on.

There can also be materials with one plane of symmetry in the xy-plane and for this thesis this shear modulus is calculated as:

$$G_{xy} = \frac{E_L}{2(1 + \nu_{LT})} \tag{2.11}$$

where the only difference to G_{TT} is the elastic modulus.

The inverse rule of mixture may also be used to calculate the in-plane shear modulus, G_{LT}, for a material with unknown reinforcement where the stiffness moduli are changed to the shear moduli as:

$$G_{LT} = \left(\frac{V_f}{G_f} + \frac{V_m}{G_m} \right)^{-1} \tag{2.12}$$

2.1.2.3 Poisson's ratio

The rule of mixtures can be used to calculate the major Poisson's ratio, ν_{LT}, according to Equation 2.13. Major Poisson's ratio is the negative of the ratio between transverse and longitudinal strain.

$$\nu_{LT} = \nu_f V_f + \nu_m V_m \tag{2.13}$$

Where ν_f and ν_m are the Poisson's ratio of the fibre and matrix, respectively.

The minor Poisson's ratio is instead calculated as:

$$\nu_{TL} = \nu_{LT} \frac{E_T}{E_L} \tag{2.14}$$

2.1.3 Thermal properties

A composite material will be affected by temperature. The calculation of the thermal properties that are explained below are the density (ρ), specific heat capacity (C_p) coefficients of thermal expansion (α), thermal strains (ε^T) and thermal conductivity (k).

2.1.3.1 Density

The density, ρ_c, of a composite material is calculated using the rule of mixtures according to:

$$\rho_c = \rho_f V_f + \rho_m V_m \tag{2.15}$$

where ρ_f and ρ_m are the densities of the fibre and matrix, respectively.

2.1.3.2 Specific heat capacity

As a composite is made from different constituents, the total specific heat capacity ($C_{p,c}$) needs to be calculated considering the properties of the constituents. The specific heat is calculated according to the rule of mixtures as:

$$C_{p,c} = C_{p,f} V_f + C_{p,m} V_m \tag{2.16}$$

where $C_{p,f}$ and $C_{p,m}$ are the specific heat capacity of the fibre and matrix, respectively.

2.1.3.3 Thermal expansion

A change in temperature of a composite will either make the material expand or shrink. This expansion/shrinkage is determined by the coefficient of thermal expansion which is different depending on the direction [7] for a unidirectional material; longitudinal (α_L) and transverse (α_T) direction. These are calculated as:

$$\alpha_L = \frac{1}{E_L}(\alpha_f E_f V_f + \alpha_m E_m V_m) \tag{2.17}$$

$$\alpha_T = (1+\nu_f)\alpha_f V_f + (1+\nu_m)\alpha_m V_m - \alpha_L \nu_{LT} \tag{2.18}$$

where α_f and α_m are the coefficient of thermal expansion of fibre and matrix, respectively.

2.1.3.4 Thermal strains

The thermal strains in the lamina are calculated considering the thermal expansions. The strains in longitudinal and transverse directions are calculated according to Equation 2.19. The strains will be the same in all direction only if the thermal expansion is isotropic.

$$\boldsymbol{\varepsilon}^T = \boldsymbol{\alpha}\Delta T \tag{2.19}$$

Here ΔT the difference between the surrounding temperature and temperature inside material.

2.1.3.5 Thermal conductivity

Thermal conductivity in the longitudinal direction (k_L) is calculated using the rule of mixtures as:

$$k_L = V_f k_f + V_m k_m \tag{2.20}$$

where k_f and k_m are the thermal conductivity of the fibre and matrix, respectively.

Thermal conductivity in the transverse direction (k_T) for fibre-reinforced materials is calculated using the Halpin-Tsai model as:

$$k_T = \frac{1 + \xi \eta V_f}{1 - \eta V_f} k_m \tag{2.21}$$

$$\eta = \frac{\frac{k_f}{k_m} - 1}{\frac{k_f}{k_m} + \xi} \tag{2.22}$$

where ξ is defined as

$$\log \xi = \sqrt{3}\ \log \frac{a}{b} \tag{2.23}$$

which gives $\frac{a}{b} = 1$ for circular fibres.

The thermal conductivity for particle-reinforced materials is calculated using the Nielsen model [8]. This is defined as:

$$k_c = k_m \left(\frac{1 + A \eta_N V_f}{1 - \psi \eta_N V_f} \right) \tag{2.24}$$

where $A = 1.5$ for spherical particles and η_N is defined as:

$$\eta_N = \frac{\frac{k_f}{k_m} - 1}{\frac{k_f}{k_m} + A} \tag{2.25}$$

and ψ is defined as:

$$\psi = 1 + \left(\frac{1 - \phi_{max}}{\phi_{max}^2} \right) \tag{2.26}$$

where $\phi_{max} = 0.7405$ for spherical particles.

As for the case for elastic and shear moduli, the inverse rule of mixtures is used to calculate the transverse thermal conductivity for the pouch-bag material. It is defined as:

$$k_T = \left(\frac{V_f}{k_f} + \frac{V_m}{k_m} \right)^{-1} \tag{2.27}$$

2.2 Battery

The general definition of a battery is a device that can store chemical energy while also transform it into electrical energy. Batteries can be divided into two categories;

single-use and rechargeable, also known as primary and secondary cells [9]. In a primary cell, the reaction inside the battery cannot be reversed and therefore only be used until fully discharged. In a secondary cell, the reactions in the cell can be reversed and hence the cell can be recharged [9].

2.2.1 Lithium-ion batteries

This project focuses on secondary lithium-ion (Li-ion) battery chemistry. A regular Li-ion battery cell has six main constituents; a positive electrode, a negative electrode, a positive current collector, a negative current collector, electrolyte and a separator.

A basic schematic sketch of a secondary Li-ion battery cell under discharge can be found in Figure 2.2. The two red rectangles represent the negative electrode and current collector, and the two green rectangles represent the positive electrode and current collector. The yellow, wavy rectangle in the middle represents the electrolyte and the blue the separator. The external circuit runs between the current collectors where the electrons travel through the external device, powered by the battery cell.

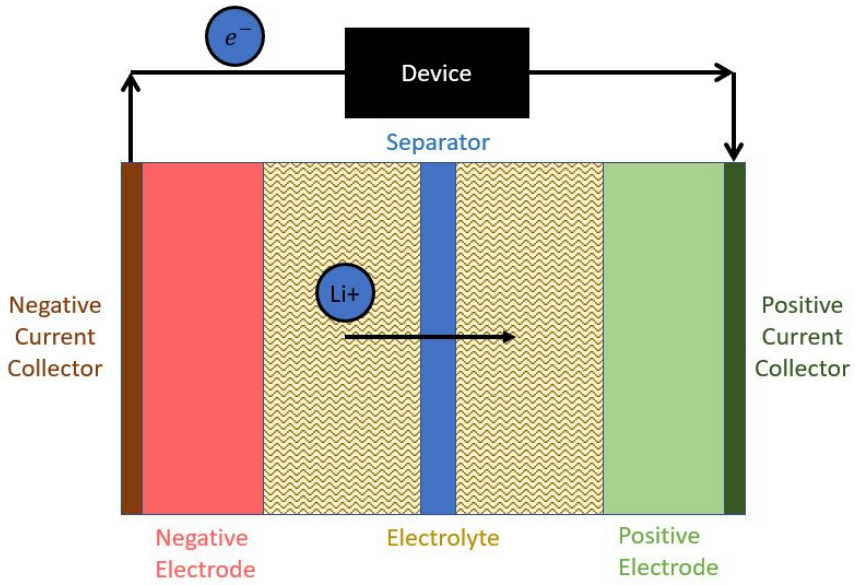

Figure 2.2: Schematic illustration showing the basics of a battery cell under discharge. Under charge, the current (illustrated by arrows) will change direction and go from positive to negative.

The energy in a secondary battery cell comes from the movement of electrons which travels from the negative to the positive electrode via an external circuit [9]. The electrons can move as there are reduction-oxidation reactions (also called redox reaction) present [9]. The electrodes contain an active material that can convert stored chemical energy to electrical energy under these chemical reactions [10]. The func-

tion of the current collectors, which are in contact with the different electrodes, is to enable the electrons to move from the active material in one electrode to the other in an efficient manner [11]. To balance the movement of the electrons there are charged ions that migrate between the electrodes inside the electrolyte [9]. In the electrolyte, the separator is present which allows the ions to pass through while it separates the electrodes from each other [10]. If the electrodes come into contact, there will be an electrical shorting of the battery [10]. When the battery is fully discharged, an external energy source is added which reverses the reaction as the current moves in the opposite direction to recharge the battery [10].

The negative electrode in a conventional Li-ion battery cell is often made of graphite while the positive electrode is made of metal based materials. Both electrodes are porous and in addition to the active electrode particles, binder material and conductive additives are added to improve the electrical conductivity and mechanical integrity of the electrodes. The porous electrodes and separator are soaked in liquid electrolyte to enable Li-ions to move between the active electrode materials. The positive electrode particles can be some form of NMC (lithium-manganese-cobalt-oxide) or LFP (lithium iron phosphate) [11]. The reason that a porous electrode is used is that it reduces energy losses and hence increases the efficiency of the electrode [11].

The current collectors in a Li-ion battery are made of copper on the negative side and aluminium on the positive side [11]. The separator is usually made from some type of reinforced polymer; either by using glass fibre or ceramics.

2.2.1.1 Pouch-cell

In the scope of this thesis, the battery cell will be placed in a pouch-bag. A pouch-cell is a laminated cell that is concealed inside a thin layer of insulating material formed as a pouch. The pouch-bag is made from a laminated material and acts as a barrier against oxygen and moisture, which if in contact with the battery cell can cause damage [12]. Figure 2.3 shows an example of a pouch-cell.

In the scope of this thesis, the pouch-bag material used was a laminated material with PET (polyethylene terephthalate), aluminium and PE (polyethylene) [12]. The thicknesses of these material was 12/9/75 [μm] [12], respectively.

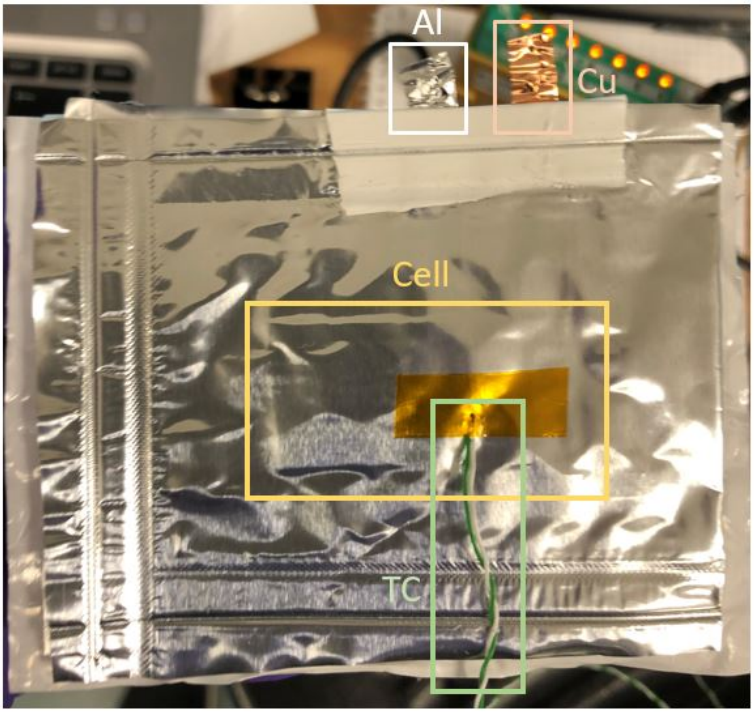

Figure 2.3: Example of a pouch-cell. In this example the aluminium (white) and copper (light brown) current collectors are visible outside the pouch-bag and the contours of the cell (yellow) is visible through the pouch-bag. There is also a thermocouple (green) attached on the outside. Thermocouples are used to study the temperature changes in the cell.)

2.2.2 Thermal properties

A battery will heat up or cool down during electrochemical cycling (i.e. charging/discharging of the battery). This heat generation/absorption is dependent on different factors like the temperature in the surrounding environment, discharge rate, internal resistance, etc.

C-rate is a measurement that relates the charge/discharge rate current of a battery to its rated capacity. In this measurement, 1C means that the battery will discharge fully in one hour and for example, 2C and 0.5C mean discharge in 30 minutes and 2 hours respectively.

State of charge (SOC) is the percentage of capacity available with respect to the rated capacity of the battery cell [13]. SOC of the battery is between 0 and 1, where the lower value means that the battery is completely discharged and the higher means fully charged [13]. Analyses by Lu et al. [14] show that more heat is generated when a battery is charged/discharged at a high C-rate as well as at low state-of-charge.

Associated with heat generation in Li-ion batteries are some risks to consider like thermal runaway, which is a phenomenon where increased temperature changes the

conditions of the battery in such a way that the temperature keeps increasing [11]. Thermal runaway can lead to fire or explosion [11].

2.2.3 Diffusion induced strains

The battery, if it works correctly, will not be affected by hygroscopic strains as one cannot allow any moisture inside the battery cell as this will result in lost electrochemical functionality. Instead, there will be electrochemical strains which cause a volume change in the battery electrodes or shrinkage during charge/discharge cycle [5]. These strains are calculated considering the normalised lithium concentration in the active material inside the electrodes [5]. This normalised concentration is calculated as:

$$\hat{C} = \frac{C}{C_{sat}} \tag{2.28}$$

where C is the concentration and C_{sat} is the saturated concentration (maximum possible concentration) of lithium [5].

The electrochemical strains can then be calculated as:

$$\boldsymbol{\varepsilon}^E = \boldsymbol{\beta}\Delta\hat{C} \tag{2.29}$$

where $\Delta\hat{C}$ is the difference in concentration and $\boldsymbol{\beta}$ is the expansion coefficient for hygroscopic-like electrochemical expansion [5].

2.3 Structural battery composite

A structural battery composite is a combination of a composite and battery, i.e. a device that can carry load while also store electrical energy. There are, as of present day, two different types of structural batteries under development, the 3D battery and the laminated battery [1] where the latter is the focus of this thesis. The basics of the laminated battery are that composites and batteries have a similar structure where both are made of different layers [1]. The laminated structural battery cell, in this thesis, is made of the same constituents as an ordinary battery cell but each constituent can also carry load, instead of only being electrochemically active or electrically conductive.

The negative electrode in the laminated structural battery cell is changed from graphite to carbon fibre compared to a regular Li-ion battery. This substitution is possible as carbon fibres have similar properties regarding intercalation of Li-ions but do also have better mechanical properties [1] which makes them a better fit in a structural battery. The carbon fibre must be combined with an electrolyte that can both transfer load and provides ion conduction [15]. This is often not the case for electrolytes used in regular battery cells as these often use liquid electrolytes, which do not give mechanical advantages [15]. The electrolyte used in structural battery composites will therefore be some type of structural battery electrolyte (SBE), which

refers to an electrolyte which has both mechanical and electrochemical properties.

The concept of SBE is relatively new as this sort of electrolyte has not been needed before the evolution of structural batteries [15, 16]. There have been studies on different approaches on how to make the best possible SBE [16]. The most promising approach to date seems to be the use of heterogeneous electrolytes that combines two different material phases, e.g. solids and liquids [16]. In these the liquid phase provides good ion conductivity, i.e. allows the ions to move through the material, while the porous polymer matrix (some type of thermoset) provides good mechanical properties [16].

The positive electrode is made from commercial Li-ion battery (see chapter 2.2.1) electrode film together with the same SBE as for the negative electrode. In this case, the film is made of aluminium that is coated with LFP particles, carbon black and a PVDF binder.

Between the two electrodes, there is a separator that has the same function as a regular Li-ion battery i.e. separating the electrodes from each other [1]. As mentioned before, the separator will also be able to carry load [1]. The materials in the current collectors are the same as in an ordinary Li-ion battery cell, i.e. copper and aluminium [1].

A conceptual sketch of the whole structural battery cell can be found in Figure 2.4, showing every constituent and how these are placed.

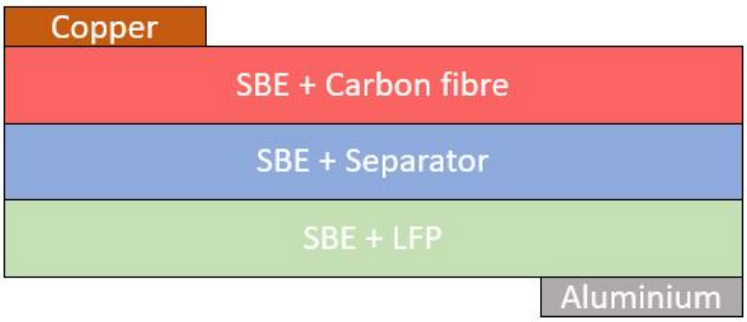

Figure 2.4: Conceptual sketch over the structural battery used in the scope of this project.

2.3.1 Strains

The total strains in the structural battery will be the added mechanical, thermal strains (Equation 2.19) extracted from laminate theory and the electrochemical analysis (Equation 2.29). The thermal and electrochemical strains will point opposite the mechanical strains. This then gives the full strain equation as:

$$\boldsymbol{\varepsilon} = \boldsymbol{\varepsilon}^M - \boldsymbol{\varepsilon}^T - \boldsymbol{\varepsilon}^E = \boldsymbol{\varepsilon}^M - \boldsymbol{\alpha}\Delta T - \boldsymbol{\beta}\Delta\hat{C} \tag{2.30}$$

where $\boldsymbol{\varepsilon}^M$ is the mechanical strains, $\boldsymbol{\varepsilon}^T$ is the thermal strains and $\boldsymbol{\varepsilon}^E$ is the electrochemical strains.

2.4 Computational framework

The finite element (FE) software COMSOL version 5.5 is used to develop the computational framework for analysis of the thermo-mechanical behaviour. This software is used for its advantages in multiphysics problems that provide a possibility to couple different physics together.

COMSOL solves models with the use of the finite element method (FEM). FEM is used to numerically calculate approximated solutions to partial differential equations (PDE) [17]. The dependent variables, in this case $\boldsymbol{u}$, in the PDE are approximated as:

$$\boldsymbol{u} \approx \boldsymbol{u}_h = \sum_{i=1}^{n} N_i a_i \tag{2.31}$$

where N_i is ith the basis function, a_i is the ith unknown variable and n is number of nodes the problem is divided into.

To be able to solve a thermo-mechanical problem, there will be need to solve two different FE-problems; one for the thermal part and one for the mechanical part. The thermal problem will use the thermal balance equation, where the unknown variable is the temperature. The mechanical problem, on the other hand, will use the momentum balance equation where the unknown variables are the displacements. The difference between these are explained in section 2.4.1 and 2.4.2 below. These two problems are coupled together to calculate the thermo-mechanical behaviour. How this is done in COMSOL is explained in section 2.4.3.

2.4.1 Thermal balance equation

The general thermal balance equation is described as:

$$\rho C_p \frac{dT}{dt} + \boldsymbol{q} \cdot \nabla = Q_{gen} \tag{2.32}$$

where ρ is density, C_p the specific heat capacity, T the temperature, Q_{gen} the generated heat e.g. due to electrochemical processes and the $\boldsymbol{q}$ the heat flux vector.

The heat flux vector ($\boldsymbol{q}$) for diffusion in a solid is described according to Equation 2.33, which is also called Fourier's law.

$$\boldsymbol{q} = -k\nabla T \tag{2.33}$$

where k is the thermal conductivity and ∇T the temperature change with respect to direction.

The thermal balance equation can therefore be updated to:

$$\rho C_p \frac{dT}{dt} + \nabla \cdot (-k\nabla T) = Q_{gen} \tag{2.34}$$

2.4.1.1 Stationary

If steady state is assumed, the time derivative of the temperature in Equation 2.34 disappears. This gives the strong format of the problem in a domain Ω as:

$$\nabla \cdot (-k\nabla T) = Q_{gen} \; in \; \Omega \tag{2.35}$$

There is also some boundary conditions needed in order to solve the problem later on. Commonly used boundary conditions are described for temperature and heat exchange, illustrated by the examples in Equations 2.36-2.38. Boundary condition 1, Equation 2.36, states a prescribed temperature T_0 on boundary Γ_1. Boundary condition 2, Equation 2.37, states the heat exchange with surrounding by convection on Γ_2. Boundary condition 3, Equation 2.38, states no heat exchange with surrounding on Γ_3.

$$T = T_0 \; on \; \Gamma_1 \tag{2.36}$$

$$(-k\nabla T) \cdot \boldsymbol{n} = h(T_{ext} - T) \; on \; \Gamma_2 \tag{2.37}$$

$$(-k\nabla T) \cdot \boldsymbol{n} = 0 \; on \; \Gamma_3 \tag{2.38}$$

where h is the heat transfer coefficient, T_{ext} the external temperature i.e. temperature of the surrounding, T the calculated temperature on the boundary and Γ_i the different boundaries.

The strong form, Equation 2.35, is transformed into the weak form. The strong form is multiplied with a testfunction (v) and integrated over the domain Ω on both sides, which results in Equation 2.39 [17].

$$\int_\Omega v\nabla \cdot (-k\nabla T) \; d\Omega = \int_\Omega vQ_{gen} \; d\Omega \tag{2.39}$$

Integration by parts, Equation 2.40, is used to rewrite this formulation to the weak form.

$$\int_a^b u(x)v'(x)dx = [u(x)v(x)]_a^b - \int_a^b u'(x)v(x)dx \tag{2.40}$$

where $u(x)$ and $v(x)$ are variables and a, b the boundary.

The resulting weak form for a stationary thermal problem then is:

$$\int_\Omega k\nabla T \cdot \nabla v d\Omega + \int_\Gamma v(-k\nabla T) \cdot \boldsymbol{n} d\Gamma = \int_\Omega vQ_{gen} d\Omega \tag{2.41}$$

The thermal balance equation can be transformed by discretization, using Galerkin method together with the weak form, to form a solvable numerical equation [17]. The discretization was explained in Equation 2.31, where $\boldsymbol{u}$ in this case is the temperature, T.

The discretized equation is described as Equation 2.42, where T has been changed to the approximated temperature [17]. The unknown variables are the n number of approximated temperatures T_i.

$$\sum_{i=1}^{n} T_i \int_\Omega k\nabla N_i \cdot \nabla v dV + \sum_{i=1}^{n} \int_\Gamma (-kT_i\nabla N_i) \cdot \boldsymbol{n} v dS = \int_\Omega Q_{gen}(\sum_{i=1}^{n} T_i N_i) v dV \tag{2.42}$$

This discretized weak form is not solvable as boundary conditions are required to take away some possible solutions. The boundary conditions make it possible to rewrite the discretized weak form to the FE-form [17]. The FE-form is a solvable matrix equation and is described as:

$$\boldsymbol{K}\boldsymbol{a} = \boldsymbol{f} \tag{2.43}$$

where $\boldsymbol{K}$ is the stiffness matrix of the size nxn, $\boldsymbol{a}$ the unknown variables in a column vector (1xn) and $\boldsymbol{f}$ is the load vector (1xn).

All these steps are conducted by COMSOL when a problem is chosen and the boundaries are set. The strong form of the problems are already predefined in the software while the boundary conditions are chosen by the user. These boundary conditions affect the results depending on what is sought for. COMSOL solves the resulting FE-form by numerical iteration.

2.4.1.2 Time-dependent

If the problem is time-dependent, the derivative of temperature in the thermal balance, Equation 2.34, no longer disappears [17]. This leads to a change in the discretized weak form as there will be an extra term.

$$\rho C_p \frac{\partial T_i}{\partial t} \sum_{i=1}^{n} \int_\Omega N_i v dV + \sum_{i=1}^{n} T_i \int_\Omega k \nabla N_i \cdot \nabla v dV + \sum_{i=1}^{n} \int_\Gamma (-k T_i \nabla N_i) \cdot \boldsymbol{n} v dS = \int_\Omega Q_{gen} (\sum_{i=1}^{n} T_i N_i) v dV \tag{2.44}$$

To solve this, the time domain ($\frac{\partial T_i}{\partial t}$) can be approximated according to the method of lines [17] which gives:

$$\frac{\partial T_i}{\partial t_T} \approx \frac{T_{i,t_T+\Delta t_T} - T_{i,t_T}}{\Delta t_T} \tag{2.45}$$

where t_T denote the time.

The time-dependent problem in discretized weak form is rewritten together with boundary conditions in the same way as for the stationary case, to form the FE-form in COMSOL. COMSOL then solves this FE-form by numerical iteration.

2.4.2 Momentum balance equation

The Cauchys momentum balance equation is defined in COMSOL as:

$$\rho \frac{\partial^2 \boldsymbol{u}}{\partial t^2} = \nabla \cdot \boldsymbol{\sigma} + \boldsymbol{b} \tag{2.46}$$

where $\boldsymbol{\sigma}$ are the stresses, $\boldsymbol{b}$ are the body forces and $\boldsymbol{u}$ the displacements.

In the case of the study in this thesis, the displacement will not change with time (quasi-static conditions), which means the first term will disappear. There will also

be no body forces, as no external forces are affecting the model. This means that Equation 2.46 is simplified to:

$$\nabla \cdot \boldsymbol{\sigma} = 0 \tag{2.47}$$

Equation 2.47 is therefore the strong form of the mechanical problem. The unknown variables are the displacement field $\boldsymbol{u}$. The boundary conditions for these types of problems are usually given as prescribed displacements and tractions as:

$$\boldsymbol{u} = \boldsymbol{u}_p \; on \; \Gamma_i \tag{2.48}$$

$$\boldsymbol{t} = \boldsymbol{\sigma} \cdot \boldsymbol{n} = \boldsymbol{t}_p \; on \; \Gamma_j \tag{2.49}$$

This strong form is rewritten to FE-form, in COMSOL, using the same steps as for the thermal balance equation, i.e. multiplication with test function, integration over the domain, use integration by parts and then discretization of the weak form. The resulting discretization will depend on boundary conditions and number of elements.

2.4.3 Coupling

Figure 2.5 below shows a schematic illustration of how the different analyses of a multiphysics model are coupled to each other. The coupling terms between the thermal and mechanical analyses are the temperature (T) and the heat generated due to dissipation (Q_d) [18]. The electrochemical analysis gives the heat generated by electrochemical cycling (Q_E) to the thermal analysis and lithium concentration (c) to the mechanical analysis [18]. This Figure then explains which parameters from one analysis that will affect the other analysis and vice verse. A one-way coupling implies that one follows the arrows pointing in one direction, only.

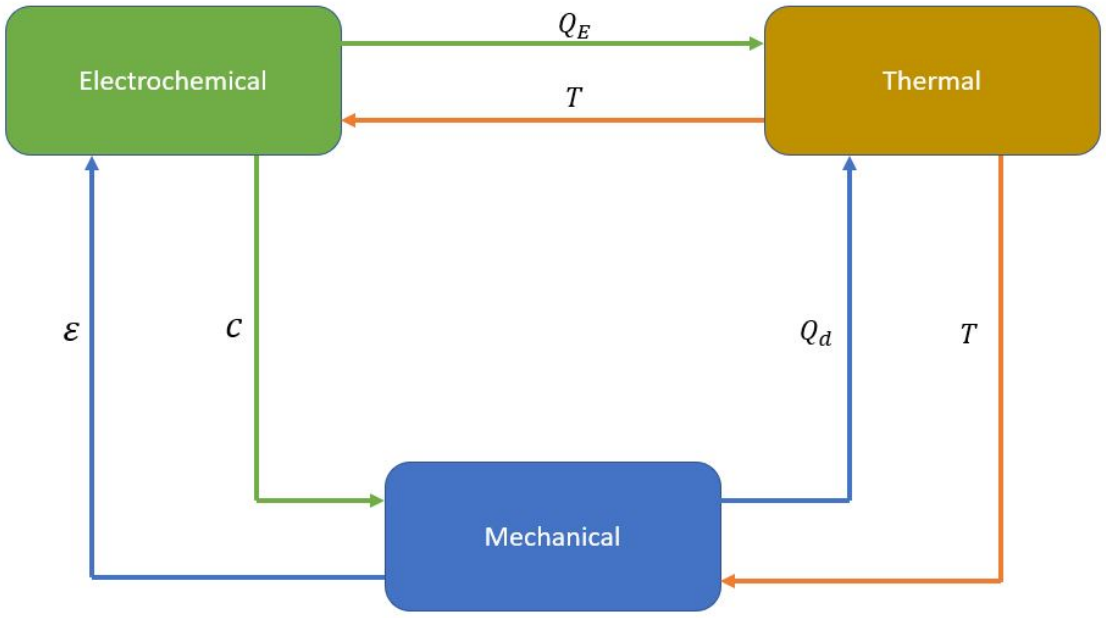

Figure 2.5: Schematic illustration of coupled analysis [18].

The coupling between the thermal and mechanical analysis needs to be included in the model. Without this coupling, the material will not be able to thermally expand, as there is no temperature change, which in turn will lead to no stress/strains in the object because of temperatures. In this thesis, the heat generated due to dissipation in the mechanical analysis will be neglected and the heat generated due to electrochemical cycling can be seen as an input value. In COMSOL this is possible by using the multiphysics function.

The multiphysics function in COMSOL for this can be solved in two different ways; either by segregated or fully coupled solution. The difference between these two is how they handle the coupled problems. The fully coupled approach solves the problem for all unknowns at the same time (one iteration) while the segregated breaks down the unknowns to smaller steps where each step is an iteration. For 3D-elements, the segregated solver is often chosen automatically, as this may be faster.

3
Methodology

The structural battery composite cell was modelled in COMSOL as a simplified three-layered laminate with the two electrodes and a separator. The pouch-bag was modelled around this cell as one layer on the top and one on the bottom. The cell was assumed as a unit cell, i.e. only a small piece of the length and width was modelled and these were of the same size. A schematic illustration of the basic model can be found in Figure 3.1 below.

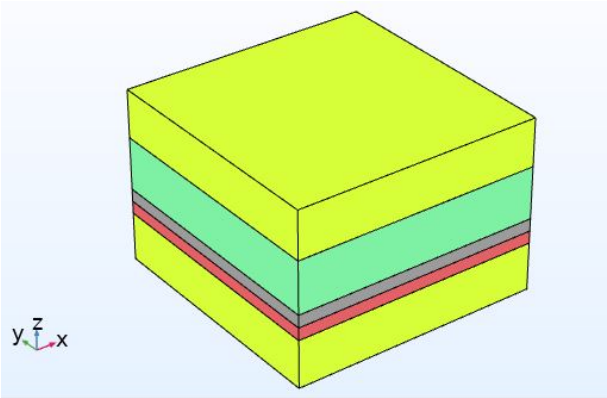

Figure 3.1: Model depicting the cell in COMSOL. The different colours represent the different layers (components); yellow is the pouch-bag, red the negative electrode, grey the separator and green positive electrode.

This chapter includes explanation on how the modelling was conducted, thermal and mechanical boundary conditions which were used and how the coupling between this model and the electrochemical model [2] was conducted.

3.1 FE-model of thermo-mechanical behaviour

The computational framework, i.e. the model, was created in the FE-software COMSOL as this enabled the important feature of coupling between thermal and mechanical physics. The battery cell was simplified to a three-layer laminate unit cell, where the current collectors were neglected. The only layers of the battery cell considered in the model were therefore the negative electrode, separator and positive electrode. The surrounding pouch-bag was modelled as a layer on the top and the bottom, respectively. This is a good representation of the entire battery pack, where the pouch-bag encloses the cell. The decision to model also the pouch-bag was made as the pouch-bag may affect the thermal behaviour of the battery cell, as it can absorb

some of the generated heat. The size of model was assumed as a unit cell, instead of using the real length and width of the battery cells.

The following general assumptions and simplifications were made in the model

- Perfect adhesion between all layers in the model
- Homogeneous applied heat source from the battery cell, i.e. the same amount of heat is applied to each of the layers in the battery cell
- The heat flux is homogeneous on the boundaries where it is applied
- The material properties are either found or assumed. The assumptions are made based on materials with similar structure or by previously conducted tests
- The materials used in the composite materials, except the carbon fibre, are isotropic. The carbon fibre is assumed to be unidirectional
- The composite materials in the electrodes and separator are all assumed to be both homogeneous and linearly elastic. These are also assumed to be unidirectional, with axis of symmetry in the yz-plane.
- The pouch-bag material is assumed to be homogeneous and linearly elastic, but orthotropic with one axis of symmetry in the xy-plane.
- The battery cell is assumed as a unit cell, with the sides in x-and y-directions having the same length, to be able to see the important through-the-thickness distribution

More detailed descriptions are provided on: how the material parameters were calculated; how the modelling was conducted; explanations of the boundary conditions; how the problem was solved; and how the coupling was made. The coupling being the one between this model and the collaborated master's thesis explained previously.

3.1.1 Material parameters

The layers in the battery cell were all different composite materials, i.e. a combination of two or more different materials. The negative electrode was chosen to be made of carbon-reinforced structural battery electrolyte (SBE), which means the material for this was a combination of carbon fibre and SBE with volume fraction of fibre $V_f = 0.4$.

The positive electrode was a porous electrode conatining $LiFePO_4$ particles, carbon black particles and PVDF binder, together with the SBE on aluminium film. For the model, this was simplified to be the combination of the LFP particles and SBE. The carbon black particles, binder and aluminium film were neglected. The volume fraction of the particles was set to $V_p = 0.48$.

The separator was made of glass-fibre reinforced SBE, which, in the model, was simplified to only have the material properties of the SBE.

The material properties, i.e. carbon fibre, SBE and $LiFePO_4$, for each of the needed

constituents can be found in the Appendix A in Tables A.1, A.2 and A.3, respectively. Here, some material properties have been found in other works but most have been assumed.

These material properties were introduced into COMSOL as parameters in global definitions. For the battery cell there were three of these parameter-folders used, one for each layer. In each of these, all properties for each used constituents were added. Analytical functions were constructed in COMSOL for the equations required to calculate the material properties with input arguments chosen accordingly. These analytical functions were then called upon in the parameter-folder for each layer.

The analytical functions were made according to the rule of mixtures (Equations 2.1, 2.13, 2.15, 2.16 and 2.20), Halpin-Tsai model (Equations 2.2 and 2.21), Nielsen model (Equation 2.4 and 2.24), minor Poisson's ratio (Equation 2.14), shear modulus in symmetry plane (Equation 2.10) and equations for longitudinal and transverse thermal expansion (Equation 2.17 and 2.18). The inputs in these are dependent on which output is sought.

The resulting material properties for the negative electrode, separator and positive electrode can be found in Table 3.1 below together with a description of each parameter and equation number.

Table 3.1: Lamina properties for the different layers in the battery cell. The first column show the parameters, the second to fourth are the different layers (negative electrode, separator and positive electrode) together with the equations used.

Parameter	**Neg (Eq.)**	**Sep (Eq.)**	**Pos (Eq.)**	**Description**
E_L [GPa]	118 (2.1)	0.535 (2.1)	2.20 (2.4)	L elastic modulus
E_T [GPa]	1.43 (2.2)	0.535 (2.2)	2.20 (2.4)	T elastic modulus
G_{LT} [GPa]	1.93 (2.8)	1 (2.8)	0.824 (2.10)	Shear modulus
G_{TT} [GPa]	0.546 (2.10)	0.194 (2.10)	0.824 (2.10)	Shear modulus yz-plane
ν_{LT} [-]	0.308 (2.13)	0.38 (2.13)	0.332 (2.13)	Major Poisson's ratio
ν_{TL} [-]	0.00373 (2.14)	0.38 (2.14)	0.332 (2.14)	Minor Poisson's ratio
ρ_c [kg/m^3]	1400 (2.15)	1100 (2.15)	2300 (2.15)	Density
C_p [J/(gK)]	1680 (2.16)	2300 (2.16)	1916 (2.16)	Specific heat capacity
α_L [10^{-6}/K]	9.98 (2.17)	2 (2.17)	1 (2.17)	L thermal expansion coeff.
α_T [10^{-6}/K]	-1.68 (2.18)	2 (2.18)	1.72 (2.18)	T thermal expansion coeff.
k_L [W/(mK)]	20.6 (2.20)	1 (2.20)	3.8335 (2.24)	L thermal conductivity
k_T [W/(mK)]	2.25 (2.21)	1 (2.21)	3.8335 (2.24)	T thermal conductivity

Moreover, there were some additional input parameters, which were needed in the model but did not have to be calculated. These parameters include the chosen width and length of the unit cell and are listed in Table 3.2 below. The heat transfer coefficient is assumed according to the one which can usually be achieved in an experimental environment.

Table 3.2: Additional parameters for the battery cell.

Parameter	**Value** [Unit]	**Description**
w	500 [μm]	Width of unit cell
l	500 [μm]	Length of unit cell
t_{neg}	25 [μm]	Thickness of neg. electrode
t_{sep}	25 [μm]	Thickness of separator
t_{pos}	105 [μm]	Thickness of pos. electrode
h	5 [W/(m^{2}K)]	Heat transfer coefficient of air
T_{ext}	20 [°C]	External temperature

3.1.1.1 Pouch-bag material

The three materials used for the pouch-bag was as described previously; PET, aluminium and PE where the thicknesses was given as 12/9/75 [μm] [12], respectively. The properties of these however was not given. Therefore, approximations were made. Material properties were found in COMSOL's material library for aluminium and PE, and online for PET [19]. These properties can be found in Tables A.4, A.5 and A.6 in the Appendix A.

This particular material had, as mentioned, three constituents instead of two as was the case for the composite materials in the battery cell. One of the phases in the material was assumed to be the PET and PE merged together and the second phase the aluminium. The material was assumed as orthotropic with one axis of symmetry, in this case the xy-plane. As this material was another type of composite material, the choice was made to denote the material parameters as in-plane and out-of-plane properties. The pouch-bag was therefore not calculated using the exact same approach as for the layers in the battery cell.

The volume fraction of each constituent was identified as these were not explicitly given. The volume fraction was calculated using the thickness of each constituent relative to a total thickness. The resulting equations for the three volume fraction can be found below in Equations 3.1, 3.3 and 3.2.

$$V_{PET} = \frac{t_{PET}}{t_{PET} + t_{PE}} \tag{3.1}$$

$$V_{PE} = \frac{t_{PE}}{t_{PET} + t_{PE}} \tag{3.2}$$

$$V_{Al} = \frac{t_{Al}}{t_{PET} + t_{Al} + t_{PE}} \tag{3.3}$$

where t are the thickness of each constituent.

For the pouch-bag, the inverse rule of mixtures was assumed to be sufficient. The in-plane properties, i.e. in the x-y plane, was calculated using the equations for longitudinal properties. The shear modulus in-plane was calculated using Equation 2.10 instead of the inverse rule of mixtures because of symmetry. The out-of-plane

properties, on the other hand, was calculated using the transverse property equations with shear modulus calculated according to the inverse rule of mixtures. Poisson's ratio was assumed to be the same for the in-plane and out-of-plane directions.

The resulting material properties for the pouch-bag can be found in Table 3.3 together with the equations used for the calculations.

Table 3.3: The material properties of the pouch-bag. The fifth column denotes which equations that was used to calculate the value.

Parameter	**Value** [Unit]	**Description**	**Eq.**
E_x	7.71 [GPa]	In-plane elastic modulus	2.1
E_z	1.21 [GPa]	Out-of-plane elastic modulus	2.7
G_{xy}	2.78 [GPa]	In-plane shear modulus	2.11
G_{xz}	0.880 [GPa]	Out-of-plane shear modulus	2.12
ν_{xy}	0.393 [-]	In-plane Poisson's ratio	2.13
ρ	1152 [kg/m^3]	Density	2.15
C_p	1718 [J/(gK)]	Specific heat capacity	2.16
α_x	$3.81 * 10^{-5}$ [1/K]	In-plane thermal expansion coeff.	2.17
α_z	$1.72 * 10^{-4}$ [1/K]	Out-of-plane thermal expansion coeff.	2.18
k_x	22.6 [W/(mK)]	In-plane thermal conductivity	2.20
k_z	0.388 [W/(mK)]	Out-of-plane thermal conductivity	2.27

3.1.2 Modelling

The model of the battery cell was simplified to three different material volumes that each represent one layer (see Figure 3.1 inside the yellow pouch-bag); the positive and negative electrode, and the separator in between. These were chosen to be modelled in a 3D space, as to mirror the reality as much as possible. The geometries were stacked on top of each other to form a cuboid i.e. the cell. The width and depth of the layers were the same but the thicknesses differed according to Table 3.2.

The layers were assigned different global materials corresponding to the material parameters in Table 3.1. The density and the specific heat capacity were denoted as scalars while the other parameters were denoted in matrix-form. The way the material properties was assigned in these can be found in equations in Appendix B.1.

The two physical aspects considered in the current analysis of the structural battery were heat transfer of solids and solid mechanics. The heat transfer of solids can then solve the thermal distribution while the solid mechanics physics solves the mechanical behaviours. These two together give the possibility to simultaneously examine the thermal expansion through multiphysics considerations.

For each material volume of the battery cell, a solid domain was assigned for the heat transfer physics consideration. These solid domains use Equation 2.34 to numerically solve the heat transfer problem. A heat source domain (Q_0) was assigned to all the layers. This heat source can either come from the other model depicting

the battery part of the structural battery composite or as an assumed value. There was also a heat flux boundary assigned in the heat transfer physics on the convective form that corresponds to Equation 2.37. How this was applied onto the model are explained in section 3.1.3.

For the solid mechanics physics, the material volumes were assigned linear elastic material domains. These material domains instead use Equation 2.46 to numerically solve the problem and assign the linear elastic properties to each layer. There was a free boundary condition added together with a prescribed displacement boundary condition, these are explained in section 3.1.3.

3.1.2.1 Pouch-bag

The pouch-bag was modelled as two new layers around the battery cell; one layer on the top and one on the bottom of the cell with a thickness corresponding to the total thickness of the material used i.e. $t_{pouch} = 96$ $[\mu m]$.

The way the material properties were assigned for the pouch-bag does not differ much from the materials in the battery cell, only that this had another plane of isotropy. The pouch-bag was assumed to be isotropic in the xy-plane, which gave a different denoting in the matrices. How these are denoted can be found in the equations in Appendix B.2.

The new geometries were assigned a solid domain in the heat transfer physics and a linearly elastic material domain in the solid mechanics physics, the same approach as for the battery cell. As the same material was used for the layers, there was no need to make two domains for each physics. The previously calculated material properties and the multiphysics were assigned to the domain in the same manner as for the battery.

The heat source was though not applied onto the pouch-bag material. In the real battery, the pouch-bag will not generate heat but instead absorb heat generated by the battery cell.

3.1.3 Boundary conditions

As the model was constructed as a unit cell, some assumptions was made for the boundary conditions. The unit cell was seen as only a small portion of the whole laminate. This led to the assumption that the structural battery composite cell can be seen as a collection of multiple unit cells in a grid pattern. For this reason, it was assumed that there can be no expansion in x-or y-direction as there will be other unit cells which counteract this movements. Consequently, the sides facing the x-direction was assigned a prescribed zero displacement in this direction and similarly the other two sides were not allowed to move in the y-direction. An other constraint needed was in z-direction. Here the choice was made to let the bottom

be constrained in z-direction. All this then gave that the battery pack will only be allowed to expand in upwards z-direction.

A heat flux was also applied on the top boundary of the model as the thermal boundary condition. This was only applied at the top as the sides would not be affected as it is in direct contact with the other unit cells.

These conditions were used both for investigations with and without pouch-bag involved.

3.1.4 Solving the problem

For both the heat transfer and solid mechanics physics, the quadratic Lagrange basis functions were used. When the two physical phenomona were coupled, the option of multiphysics came through. Here the thermal expansion coefficients were added to each of the layers, which used equation 2.19. Without this feature, there would be no stresses in the materials and the materials would not be allowed to expand.

The coupled problem was solved using the fully coupled solution. This means that both the heat transfer problem and the solids mechanics problem were solved simultaneously instead of separately.

As the solution need to be time-dependent, the study was chosen as time-dependent. The range of the time studied either came from the electrochemical model or from chosen time-steps. The results from the studies were taken as the temperature, stress and strain distribution which give the total thermo-mechanical behaviour.

A validation of the final model was conducted as explained in Appendix C which gave that both the material properties and the model gave a sufficient accurate result with the used material parameters.

3.2 Coupling

As this thesis focus on the thermo-mechanical behaviour of the structural battery composite, the electrochemical impact was not included in this model. This instead came into the model by using results regarding power dissipation density (i.e, the generated heat) from the battery model conducted by the collaborated master's thesis [2].

The total power dissipation density was available as graphs over time for different C-rates in the battery cell which in turn gives tables with time and generated heat in the two columns. These tables were then used as inputs in the heat source domains for the three layers in the battery cell by using the interpolation function in COMSOL.

4

Results and discussion

The modelling results are presented and discussed in this chapter. The model is first simulated under 180 seconds with a heat source of 500 kW/m^3 and heat transfer coefficient of 5 W/(m^{2}K) in the heat flux for temperature, strain and stress distribution, without and with the pouch-bag. Different comparisons is then conducted by changing the time-span, heat transfer coefficient (h), applied heat source and the thickness of the layers. All of these comparisons are conducted without the pouch-bag. The results are discussed directly in each section but an overall discussion is also present to tie together all the different results.

It is important to emphasise that because the analysis performed in this thesis almost exclusively considers assumed input data, the size of values are not the significant results. Instead focus is on the identification of trends and how different parameters affects the overall behaviour of the structural battery cell. Consequently, how the distributions act are more important than the actual values.

4.1 Thermo-mechanical framework

The temperature, strain and stress distributions are shown in the Figures below (4.1b, 4.2, 4.3a and 4.3b) after 180 seconds with a heat source of 500 kW/m^3, pouch-bag excluded and with non-material related parameters taken from Table 3.2. These Figures are depicted for the chosen boundary conditions with heat flux only applied at the top and the three other sides are locked in displacement as explained in the methodology section 3.1.3. The heat transfer coefficient in the heat flux is assumed to be 5 W/(m^{2}K).

Figure 4.1 shows the temperature for 0 and 180 seconds. In Figure 4.1b there has been a temperature increase which is expected. The temperature is now around 32.2°C, i.e. increase of 12.2°C. As the thickness is small compared to the width/length, the heat goes fast through the thickness and therefore the temperatures become close to uniform through the whole cell. Even if the temperature looks the same in the plot, there are small variations through the thickness.

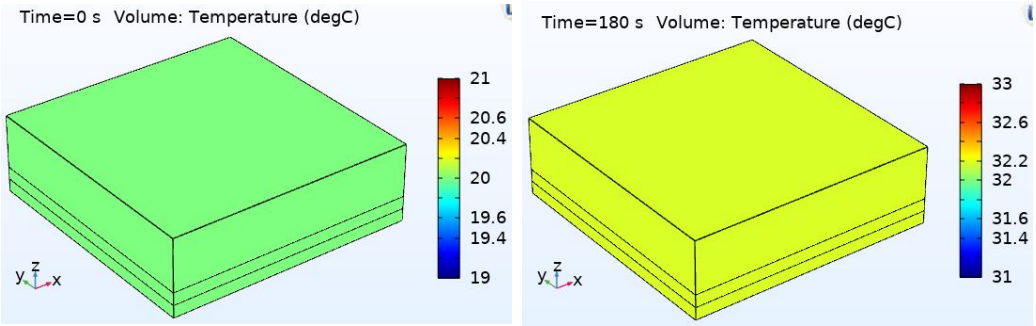

(a) Temperature at 0 seconds with the value 20°C.

(b) Temperature at 180 seconds with the value 32.2°C.

Figure 4.1: Temperature distribution in Celsius of the battery cell with heat source 500 kW/m^3 on each constituent and heat transfer coefficient 5 W/(m^{2}K).

The strain distribution in z-direction, Figure 4.2, differs according to the three layers of the battery cell where the highest strains are found in the separator while the lowest are in the negative electrode. A validation of the strains was performed as described in Appendix C, here the strains are also shown when only considering each layer separately.

The magnitudes of the strains are reasonable as the battery cell deforms with a multiple of 0.001% for each layer after 180 seconds. The displacements are locked in x-and y-direction, these strains are therefore approximately zero and not shown here.

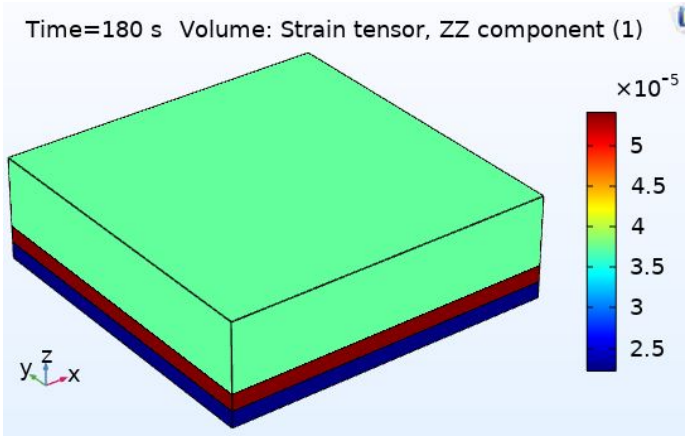

Figure 4.2: Strain distribution in z-direction of the battery cell with heat source 500 kW/m^3 on each constituent and heat transfer coefficient 5 W/(m^{2}K).

Figure 4.3 shows the stresses in both x-and y-direction. The stresses in z-direction are not depicted as these are infinitely small as the materials are allowed to move in this direction. As the bars of these graphs show, the stresses in the two directions are pointing in the relative opposite direction. For the x-direction, Figure 4.3a, the highest stresses are located in the negative electrode and are 100 times bigger than in the separator which has the lowest stresses. For the y-direction, Figure 4.9b, how-

ever, the stresses are highest in the positive electrode but the highest and lowest are of the same multiple. This means that the highest stresses overall is located in the negative electrode's x-direction. The stresses are in fact dependent on both strains and elastic modulus and fibres lies in the x-direction i.e. the highest elastic modulus.

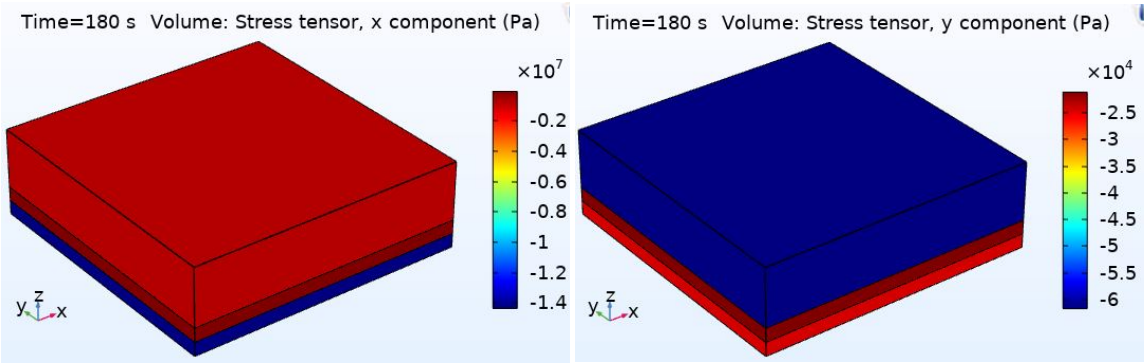

(a) x-direction **(b)** y-direction

Figure 4.3: Stress distribution in x-direction (4.3a) and y-direction (4.3b) at time 180 seconds with applied heat source 500 kW/m^3 and heat transfer coefficient 5 W/(m^{2}K).

With the pouch-bag, the response looks a bit different compared to the naked battery cell for the same thermal and mechanical boundary conditions. Figure 4.4 shows the temperature distribution, which has a lower average value (29.4 °C) compared to Figure 4.1b. This behaviour can be caused by the increased total thickness/mass of the cell as there are two more layers to heat up or that the pouch-bag absorbs some extra heat.

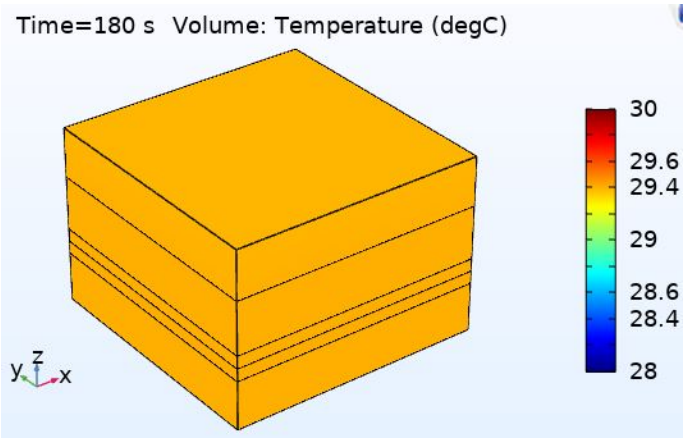

Figure 4.4: Temperature distribution of battery cell enclosed within the pouch-bag. Applied heat source of 500 kW/m^3 on each layer of the battery cell and heat transfer coefficient 5 W/(m^{2}K).

Figure 4.5 shows the strain distribution, which is higher in the pouch-bag compared to the battery cell (Figure 4.2) inside. This is due to the large thermal expansion

coefficient of the pouch-bag material (Table 3.1). The strains in the battery cell seem to have the same values because of the colouring but these actually differs relatively much. These strains are though lower than the pouch-bag and therefore lies in the same area domain according to the bar. If these strains are compared to the ones without the pouch-bag, see Figure 4.2 above, these are a bit smaller but of the same size order. It should be noted that the perfect adhesion between the pouch-bag layers and the battery cell is only assumed.

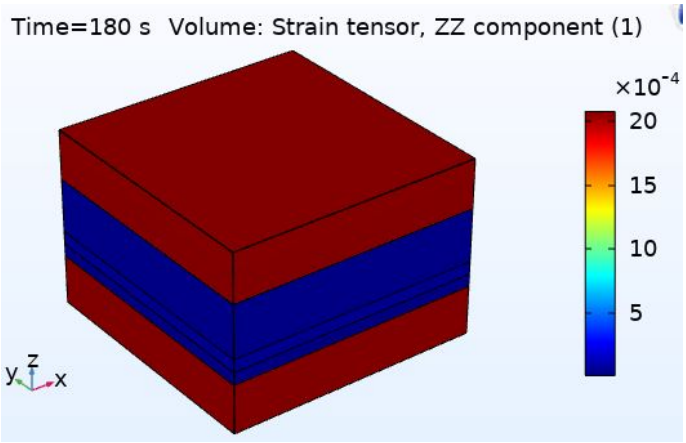

Figure 4.5: Strain distribution in z-direction of battery cell enclosed within the pouch-bag. Applied heat source of 500 kW/m^3 on each layer of the battery cell and heat transfer coefficient 5 W/(m^{2}K).

Figure 4.6 shows the stress distributions in x-and y-direction. In x-direction, Figure 4.6a, the size order of the stresses are the same compared to Figure 4.3a with the stress of the pouch-bag being second highest. The same can be seen for the y-direction stresses, Figure 4.6b, with the difference being that the pouch-bag here has the highest stresses. In both directions the stresses in the battery cell here are smaller compared to Figure 4.3 but they are of the same multiple, i.e. the same behaviour can be seen as for the strains.

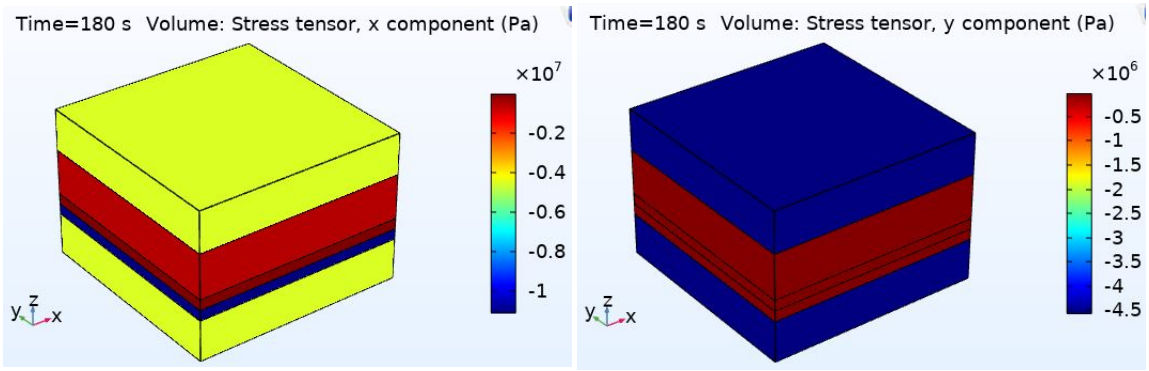

(a) x-direction **(b)** y-direction

Figure 4.6: Stress distribution of battery cell enclosed within pouch-bag in x-direction (4.6a) and y-direction (4.6b) at time 180 seconds with applied heat source 500 kW/m^3 on the battery cell.

In a real battery pack, the pouch-bag will not be layered with the battery cell but rather enclose it. Hence, the strains nor the stresses may not be transmitted directly to the pouch-bag which is the case for the model. The pouch-bag's function is not to take load but to protect the battery cell from the outside. Therefore the pouch-bag will affect the temperature distribution is expected to have limited effect on the mechanical performance. This is the main reason why the pouch-bag is neglected when conducting the sensitivity analysis below.

4.1.1 Sensitivity analysis

The time span, heat transfer coefficient, applied heat source and thicknesses of the different layers is varied to see how these affect the results. All these tests are conducted without the pouch-bag, i.e. only the battery cell is considered.

The graphs in this section are plotted in MATLAB[1] with values directly exported from COMSOL.

4.1.1.1 Time

Figure 4.7a depicts the response with no applied heat flux which shows a linear response. Without a heat flux, there is nothing counteracting the temperature increase and therefore it increases linearly over time. This makes the temperature go towards infinity if the time studied is large enough. In reality there will be some type of heat flux affecting the battery cell, as there will be differences in temperature between the battery cell and the surroundings.

Figure 4.7b depicts the response with a heat flux applied on the top of the battery cell which gives a non-linear response. The longer time the model is simulated the smaller the temperature increase becomes. The graph flattens as the response goes towards steady state, where the temperature will no longer increase.

[1] MATLAB is a programming platform with a matrix-based language [20]

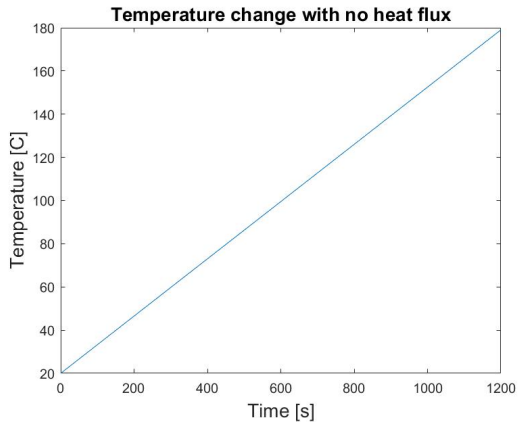

(a) No heat flux.

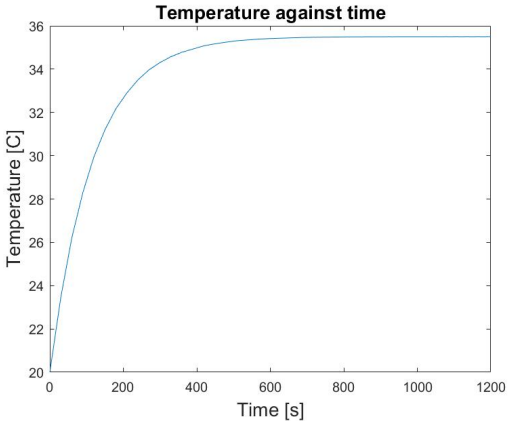

(b) Heat flux with heat transfer coefficient 5 W/(m^{2}K).

Figure 4.7: Temperature change over time in the battery cell with and without applied heat flux with applied heat source 500 kW/(m^{2}K).

Figure 4.8 shows how the strains in z-direction in the layers change over time with applied heat flux. These has a similar non-linear response as the temperature change in Figure 4.7b above. The order of the strains does not change compared to Figure 4.8 as all strains are increased with similar percentage. These results are expected as the expansions are thermally induced in z-direction and therefore the strains are directly dependent on the temperature increase.

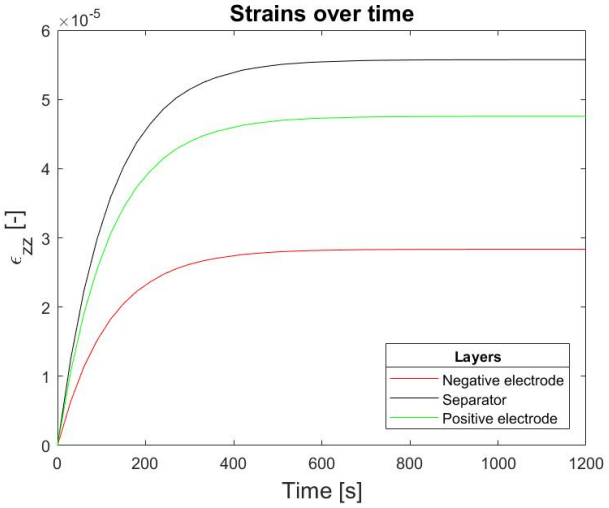

Figure 4.8: Average strain over time with heat transfer coefficient 5 W/(m^{2}K), where red represent the negative electrode, black the separator and green the positive electrode.

The stresses in x- and y-direction are shown in Figure 4.9 which, as expected, follows the same response as for the temperature. As previously mention, the stresses are directly dependent on the strains of the materials. The stresses in the positive electrode and separator are much smaller compared to the negative electrode, therefore

these lie near the x-axis of the graph in the x-direction, see Figure 4.3a.

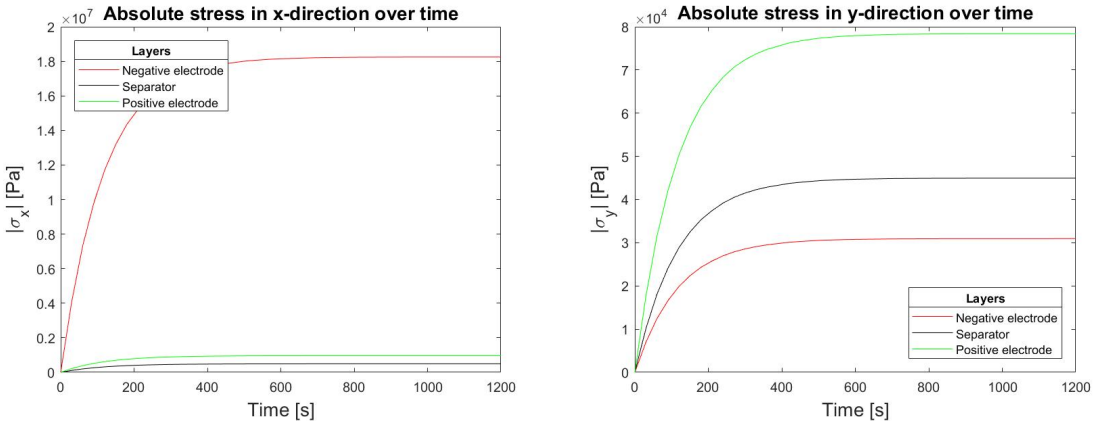

(a) x-direction **(b)** y-direction

Figure 4.9: Absolute values of stress distribution over time in x-direction (4.9a) and y-direction (4.9b) with heat source 500 kW/m^3 and heat transfer coefficient 5 W/(m^{2}K).

4.1.1.2 Heat transfer coefficients (h)

Changing the heat transfer coefficient will affect the temperature change in the battery cell, as have been shown. Figure 4.10 shows how the temperature changes at 180 seconds for increased heat transfer coefficient without the pouch-bag which shows a non-linear response where the temperature decreases with increased heat transfer coefficient. The heat transfer coefficient is not directly applied but is instead a part of the heat flux which in turn is dependent on the temperature.

A higher heat transfer coefficient will also give a lower steady state temperature, i.e. a lower maximum temperature. This response can be seen in Figure 4.11 for heat transfer coefficients between 0 and 5 W/(m^{2}K). This response is expected as it is directly coupled to Figure 4.10.

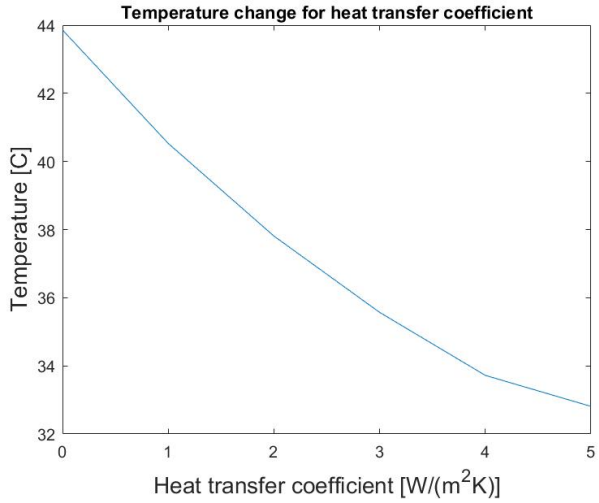

Figure 4.10: Average temperature in z-direction for different heat transfer coefficients at 180 seconds and heat source of 500 kW/m^3.

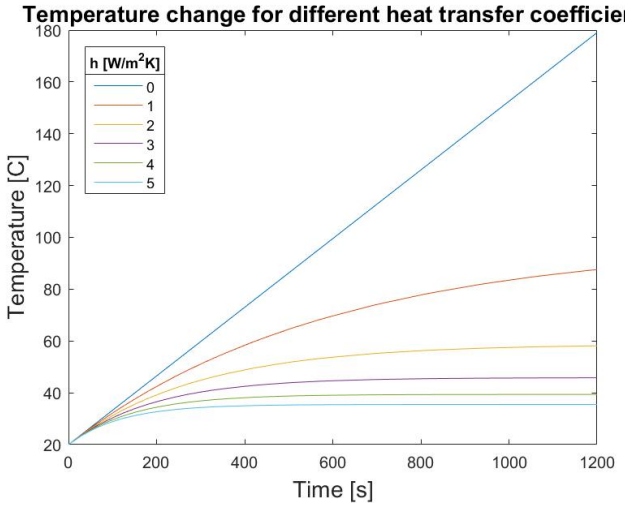

Figure 4.11: Temperature change against time for different heat transfer coefficients between 0 and 5 W/(m^{2}K) with a heat source of 500 kW/m^3.

Figure 4.12 shows how the average strains in the layers of the battery cell change with different heat transfer coefficients at time 180 seconds. As seen in the graph, the strains become smaller with higher transfer coefficients and the response has the same behaviour as for the temperature in Figure 4.10 as expected. The time response shown in Figure 4.11 can also be applied to strains, as they will act in the same manner. Even through not explicitly shown, the stresses decreases the same way.

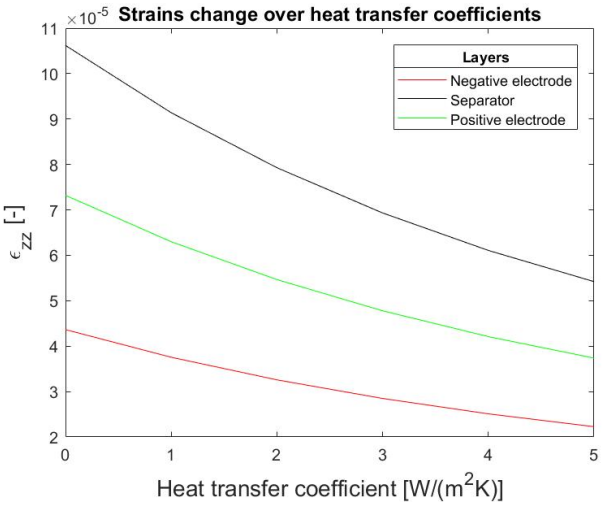

Figure 4.12: Average strains for different heat transfer coefficients for each layer with heat source 500 kW/m^3. Red line represent the negative electrode, black the separator and green positive electrode.

4.1.1.3 Heat source

When the heat source is increased, the maximum temperature will also increase as there is more heat generated in the battery cell. Figure 4.13a depicts increased heat source at time 180 seconds for the battery cell without the pouch-bag. This Figure shows that the relation between the temperature and generated heat in the battery cell is linear. As the heat source is what increases the temperature, this response is expected. As seen in previous results, this means that the strains and stresses also have linear behaviours as these are directly coupled to the temperature. The strains can be seen in Figure 4.13b below.

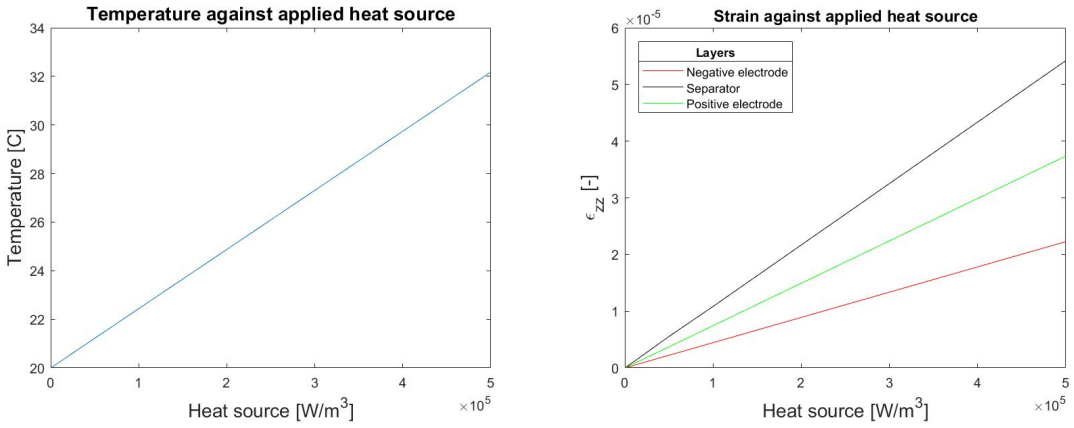

(a) Temperature against heat source. **(b)** Strains against heat source

Figure 4.13: Temperature and strains against increased heat source at time 180 seconds with heat transfer coefficient 5 W/(m^{2}K).

A important result is also how the steady state temperature changes with increased heat source. In Figure 4.14 the temperature behaviour is depicted between 1 kW/m^3

and 500 kW/m^3 with exponential steps between. The steady state is reached not so far from each other regarding time. There is however a bigger difference for the steady state temperature. For under 50 kW/m^3 is hard to distinguish the temperatures, but all these are around 20 ° C. Hence, these heat sources does not heat up the battery cell significantly.

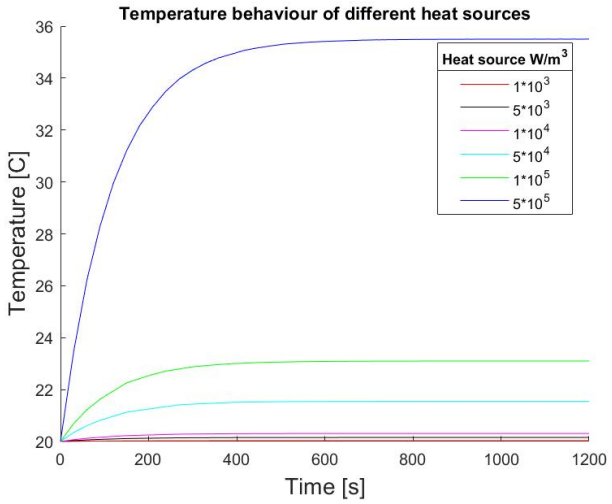

Figure 4.14: Temperature behaviour of different applied heat sources between 1 kW/m^3 and 500 kW/m^3 and heat transfer coefficient 5 W/(m^{2}K).

4.1.1.4 Thickness

How the temperature changes when the thickness is increased for each of the layers is shown in Figure 4.15. These responses are shown with heat flux applied, heat source 500 kW/m^3 and at time 180 seconds. Each layer's thickness is changed separately, i.e. when the thickness is increased for one layer, the other two stays at their respective original thicknesses (see Table 3.2). The Figure shows that the temperature increases with increased thickness which is expected as all these layers have an applied heat source. The heat source is dependent on the volume, i.e. a bigger volume of the battery cell therefore gives a higher temperature. The same responses can also be seen for the strains and stress behaviours as well.

In the Figure 4.15, increased thickness of the separator and negative electrode gives nearly the same temperature change while the positive electrode does affect it less. This can be seen as the response for the positive electrode flattens out faster than the other two and at a lower temperature. The reason for this is that the term ρC_p in equation 2.32 is larger for the positive electrode. Hence, more energy is needed to heat up the positive electrode compared with the other layers.

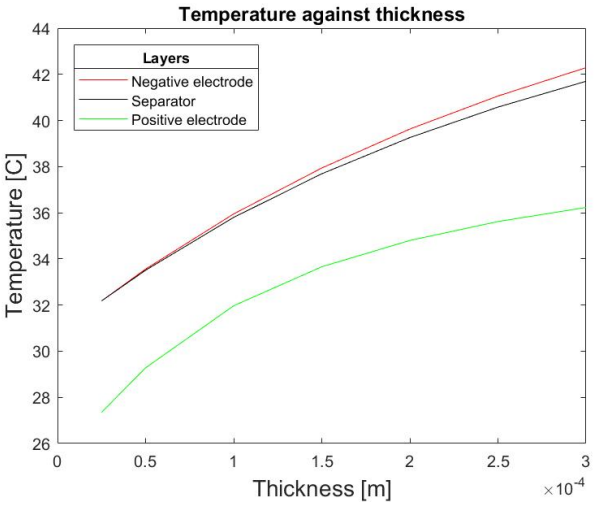

Figure 4.15: Temperature change when the thickness of each layer are change separately while the other two layers were set at its original thickness at 180 seconds, heat source 500 kW/m^3 and heat transfer coefficient 5 W/(m^{2}K).

The same approach is used to investigate the steady state for different thicknesses. In Figure 4.16 the responses are divided into three graphs, one for each layer. The thicknesses of negative electrode and separator (Figure 4.16a and 4.16b) give the same temperature change and has the same steady state. As previously stated, a thicker layer gives a higher temperature and therefore also a higher steady state temperature. Hence, the thicknesses are important but the choice to thicker either the separator or negative electrode does not matter as much as this will give a similar result.

Figure 4.16c shows the behaviour of the positive electrode. Here the temperature change is the same for all thicknesses in the beginning but after a while they change and flattens out to a steady state. The Figure still gives the same outcome as in Figure 4.15 that the temperature change is less for the positive electrode than the other two layers.

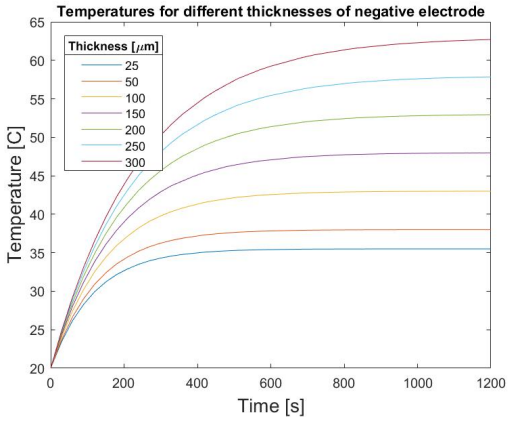

(a) Negative electrode thicknesses.

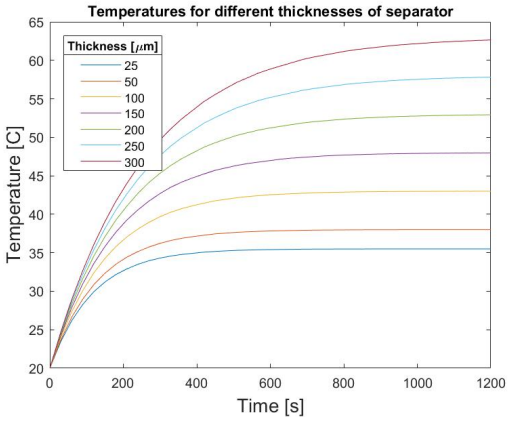

(b) Separator thicknesses.

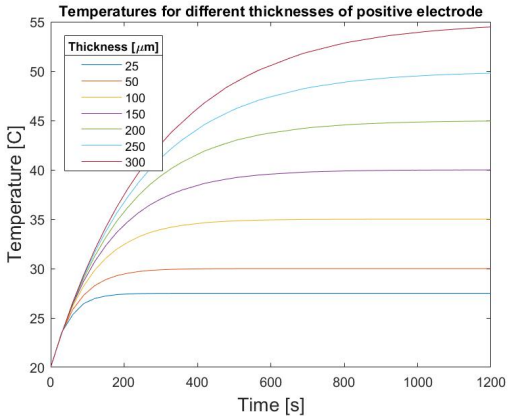

(c) Positive electrode thicknesses.

Figure 4.16: Temperature changes over time for different thicknesses of negative electrode, separator and positive electrode.

4.2 Coupled results

The resulting total power dissipation density (generated heat) from the battery cell, as explained in the methodology, comes from an other thesis [2]. The generated heat for different C-rates, in this case 1C, 3C and 5C, i.e. fully discharged after one hour (3600 seconds), 20 minutes (1200 seconds) and 12 minutes (720 seconds) are imported to the thermo-mechanical model. Figure 4.17 shows the total power dissipation density (generated heat) for these three different C-rates [2].

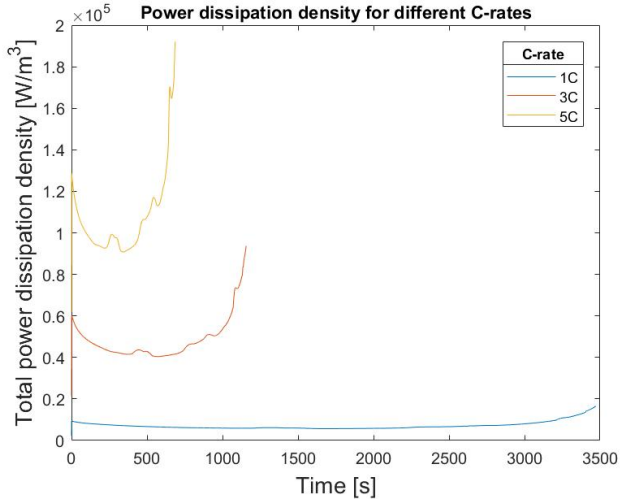

Figure 4.17: Total power dissipation density change for different C-rates from [2].

Figure 4.18 shows what happens when the total power dissipation density is applied as the input heat source in the thermo-mechanical model with the same boundary conditions as the other test and heat transfer coefficient of 5 W/(m^{2}K). Here it shows that 5C gives the highest temperature increase, as this has the highest generated heat.

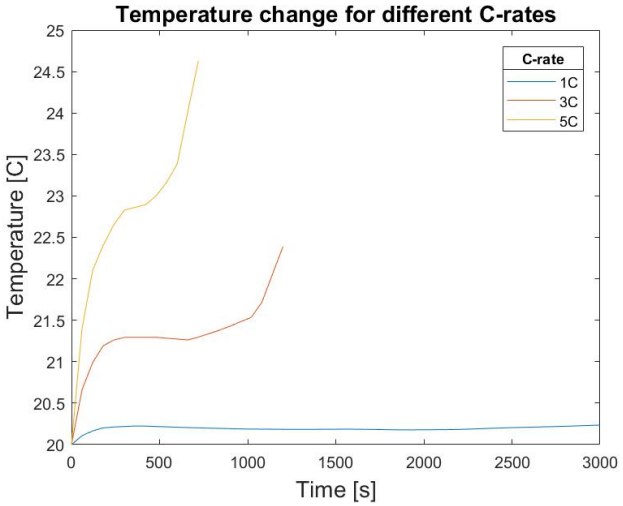

Figure 4.18: Temperature change for different input heat sources according to Figure 4.17 with heat transfer coefficient 5 W/(m^{2}K).

4.2.1 Heat transfer coefficients (h)

The heat transfer coefficient was changed to study the response of the heat source in the same way as in the sensitivity analysis above i.e., between 0 and 5 W/(m^{2}K). Figures 4.19a, 4.19b and 4.19c show the responses for each of the C-rates with these heat transfer coefficients applied to the heat flux. As described previously, 0 W/(m^{2}K) gives a linear response which goes towards infinity. Looking at the responses for the other heat transfer coefficients its clear that the higher the value

the lower the maximum temperature will be, the same as previously shown in Figure 4.11. The new thing here is that the temperatures response have multiple "bumps" instead of only one as in Figure 4.11 which is due to the heat source changing value at each time step instead of being constant as in previously tests.

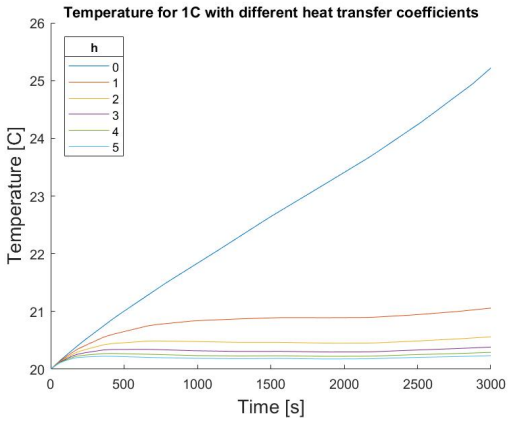

(a) Applied heat source for 1C.

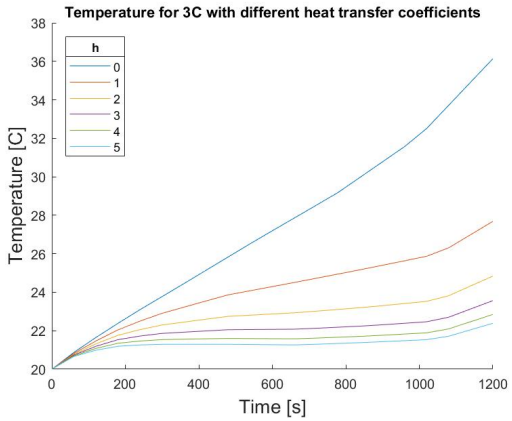

(b) Applied heat source for 3C.

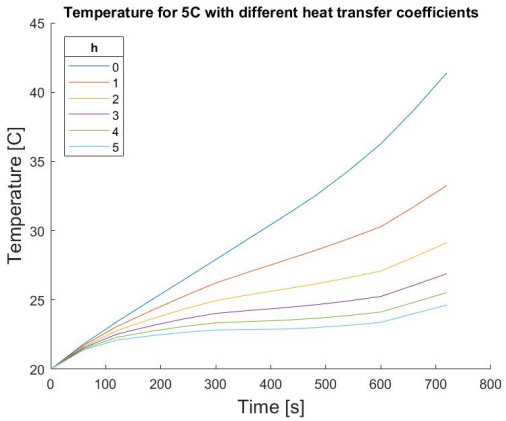

(c) Applied heat source for 5C.

Figure 4.19: Temperature changes for different heat transfer coefficients for each heat source response for different C-rates.

4.3 Overall Discussion

This thesis was not conducted the way which was originally planned as it was made under the Covid-19 pandemic where new special guidelines needed to be followed. These guidelines prohibited for multiple people to be in the lab at once, and therefore manufacturing and tests could not be performed. The the original plan was to conduct both manufacturing and testing of a structural battery composite cell with the same materials and constituents used in the modelling to see if the results can be predicted with the model. Without something to compare the results with, it is difficult to say how good the modelled framework actually predicts the results from a real test.

The original plan also involved a two-way coupling with an other master's thesis. This did not work out the way it was planned unfortunately, partly a consequence of the pandemic. Instead of a two-way full coupling there was only a one-way coupling by exchange of heat source and resulting temperature change. A two-way coupling can give a better understanding of the total behaviour as it fully connects the thermo-mechanical analysis with the electrochemical analysis. When only investigating the temperature change of the power dissipation density other behaviours are lost, for example the expansion because of the electrochemical processes. These extra expansions will affect the total expansion. Hence, this can affect the strains and stresses shown in this thesis. As these expansions are not directly coupled to the temperature in the same way as the thermo-mechanical expansions, and therefore will probably have an other behaviour pattern.

As the most of the material parameters for the materials are assumed, the resulting values can be questionable which is why this thesis focused on the behaviour of the results rather than the size of the values. There can be a parameter study on each assumed value, if wanted, but here the test were limited to time, heat transfer coefficient, heat source and thickness.

To know when the steady state temperature is reached can be important when conducting tests because steady state gives no further temperature changes. Hence, the steady state shall not be located near the surrounding temperature where the test is conducted. Knowing when the steady state is reached for different conditions may then help the tester to choose heat source (i.e. what C-rate/current to apply), how much one needs to limit the heat exchange with the surroundings (linked to the thermal boundary conditions), time for testing, etc. From these results it is clear that, for example, a too low magnitude of the heat source will make the steady state come too close to the room temperature and therefore the tests can not be performed correctly. Hence, if the heat generated from the electrochemical cycling is too low, the temperature increase may not show.

In reality there is not just a heat flux from the surroundings affecting the battery cell but also between the different components which was not considered in this thesis.

5
Conclusion and further work

The aim of this thesis was to develop a model which shows the thermo-mechanical behaviour of a structural battery composite cell. As there was no physical manufacturing and testing conducted it is not possible to say how good it predicts the reality.

The important results from this thesis instead comes from the sensitivity analysis conducted i.e. how different parameters affects the behaviour of the battery cell. This showed that a too low generated heat will lead to a low steady state. A too low steady state can possible give misleading temperatures in a future thermal test of these structural battery composite cells. It is though possible to control e.g. the generated heat by changing the C-rate in the battery cell and the heat exchange with the surroundings. Hence, the developed framework, in combination with the accompanied thesis [2], can be used to guide future experiments to study the thermal behaviour of structural batteries.

5.1 Further work

If extended studies were to be conducted on this thesis, the most important step would be to see how the materials act in a real constructed battery cell, i.e. manufacturing and testing of a battery with the same constituents. This will help show how well the model actually predicts the thermo-mechanical behaviour of this structural battery composite cell, which is what was the original plan for this thesis. This can also help show which assumptions are more accurate and which needs to be change.

Extended studies can also include fully coupling between this thermo-mechanical model and a battery model. As the structural battery composite is a combination of composites and batteries, it is important to look at all the different analysis simultaneously. This can give a more accurate modelling as fewer parameters need to be assumed and it also give all the behaviours coupled together according to figure 2.5.

Bibliography

[1] L.E. Asp, M. Johansson, G. Lindbergh, J. Xu, and D. Zenkert. Structural battery composites: a review. *Functional Composites and Structures*, 1(4):042001, Nov 2019. https://doi.org/10.1088/2631-6331/ab5571.

[2] M. Dong. Thermal analysis and battery modelling for structural battery composites. Master's thesis, Chalmers University of Technology, 2020.

[3] W. Johannisson, D. Zenkert, and G. Lindbergh. Model of a structural battery and its potential for system level mass savings. *Multifunctional Materials*, 2(3):035002, Sep 2019. https://doi.org/10.1088/2399-7532/ab3bdd.

[4] D. Carlstedt and L.E. Asp. Performance analysis framework for structural battery composites in electric vehicles. *Composites Part B: Engineering*, 186, April 2020. https://doi.org/10.1016/j.compositesb.2020.107822.

[5] D. Carlstedt. *On the multifunctional performance of structural batteries*. Licentiate thesis, Chalmers University of Technology, 2019.

[6] D. Carlstedt and L.E. Asp. Thermal and diffusion induced stresses in a structural battery under galvanostatic cycling. *Composites Science and Technology*, 179:69–78, July 2019. https://doi.org/10.1016/j.compscitech.2019.04.024.

[7] B. D. Agarwal, L. J. Broutman, and K. Chandrashekhara. *Analysis and performance of fiber composites*. John Wiley and Sons, Inc, third edition, 2015.

[8] M. Loos. Fundamentals of polymer matrix composites containing cnts. In *Carbon Nanotube Reinforced Composites*, chapter 5, pages 125–170. Elsevier Inc., 2015. https://doi.org/10.1016/B978-1-4557-3195-4.00005-9.

[9] A. Bhatt, M. Forsyth, R. Withers, and G. Wang. How a battery works, Feb 2016. https://www.science.org.au/curious/technology-future/batteries.

[10] M. Winter and J. R. Brodd. What are batteries, fuel cells, and supercapacitors. *Chemical Reviews*, 104(10):4245–4270, September 2004. https://doi.org/10.1021/cr020730k.

[11] J. T. Warner. *Lithium-Ion Battery Chemistries*, pages 43–77. Elsevier, 2019. https://doi.org/10.1016/C2017-0-02140-7.

[12] E. Jacques, M.H. Kjell, D. Zenkert and G. Lindbergh. The effect of lithium-intercalation on the mechanical properties of carbon fibres. *Carbon*, 68:725–733, March 2014. https://doi.org/10.1016/j.carbon.2013.11.056.

[13] H. Abdi, B. Mohammadi-ivatloo, S. Javadi, A.R. Khodaei, and E. Dehnavi. Energy storage systems. In *Distributed Generation Systems: Design, Operation and Grid integration*, pages 333–368. Elsevier Inc., 2017. https://doi.org/10.1016/B978-0-12-804208-3.00007-8.

[14] G. Liu, L. Lu, M. Ouyang, J. Li, and X. Han. Analysis of the heat generation of lithium-ion battery during charging and discharging considering different influencing factors. *Journal of Thermal Analysis and Calorimetery*, 116:1001–1010, May 2014. https://doi.org/10.1007/s10973-013-3599-9.

[15] N. Ihrner, W. Johannisson, F. Sieland, D. Zenkert, and M. Johansson. Structural lithium ion battery electrolytes via reaction induced phase-separation. *Journal of Materials Chemistry A*, 5:25652–25659, November 2017. https://doi.org/10.1039/C7TA04684G.

[16] L.M. Schneider, N. Ihrner, D. Zenkert, and M. Johansson. Bicontinuous electrolytes via polymerization for structural lithium ion batteries. *ACS Applied Energy Materials*, 2(6):4362–4369, 2019. DOI: 10.1021/acsaem.9b00563.

[17] The Finite Element Method (FEM). https://www.comsol.se/multiphysics/finite-element-method, February 2017.

[18] D. Carlstedt, J. Xu, K. Runesson, F. Larsson, and L.E. Asp. Unit cells for multiphysics modelling of structural battery composites., 2019. In: Proceedings of the ICCM22. Melbourne, Australia.

[19] designerdata. PET. https://designerdata.nl/materials/plastics/thermo-plastics/polyethylene-terephthalate, 2020.

[20] Mathworks. What is MATLAB. https://se.mathworks.com/discovery/what-is-matlab.html, 2020.

[21] S. Duan, F. Liu, T. Pettersson, C. Creighton and L.E. Asp. Determination of transverse and shear moduli of single carbon fibres. *Carbon*, 158:772–782, March 2020. https://doi.org/10.1016/j.carbon.2019.11.054.

[22] D.E. Bowles and S. S. Tompkins. Prediction of coefficients of thermal expansion for unidirectional composites. *Journal of Composite Materials*, 23(4):370–388, 1989. https://doi.org/10.1177/002199838902300405.

[23] Y. Qi, L.G. Hector, C. James, and K.J. Kim. Lithium concentration dependent elastic properties of battery electrode materials from first principle calculations. *Journal of The Electrochemical Society*, 161(11):3010–3018, November 2014. DOI: 10.1149/2.0031411jes.

A

Material properties

Table A.1: Material parameters of carbon fibre. Reference lack of data meaning that assumption has been made.

Parameter	Value [Unit]	Description	Ref.
$E_{f,1}$	294 [GPa]	Longitudinal elastic modulus	Lack of data
$E_{f,2}$	14 [GPa]	Transverse elastic modulus	[21]
G_f	8.78 [GPa]	Shear modulus	[21]
ν_f	0.2 [-]	Poisson's ratio	Lack of data
$\alpha_{f,1}$	$1 * 10^{-5}$ [1/K]	Longitudinal thermal expansion coeff.	[22]
$\alpha_{f,2}$	$-0.54 * 10^{-6}$ [1/K]	Transverse thermal expansion coeff.	[22]
$C_{p,f}$	0.750 [J/(gK)]	Specific heat capacity	Lack of data
ρ_f	1850 [kg/m^3]	Density	Lack of data
k_f	50 [W/(mK)]	Thermal conductivity	Lack of data
V_f	0.4 [-]	Volume fraction	Chosen value

Table A.2: Material parameters of structural battery electrolyte. Reference lack of data meaning that assumption has been made.

Parameter	Value [Unit]	Description	Ref.
E_m	0.535 [GPa]	Elastic modulus	[15]
G_m	1 [GPa]	Shear modulus	Lack of data
ν_m	0.38 [-]	Poisson's ratio	Lack of data
α_m	$2 * 10^{-6}$ [1/K]	Thermal expansion coeff.	Lack of data
$C_{p,m}$	2.3 [J/(gK)]	Specific heat capacity	Lack of data
ρ_m	1100 [kg/m^3]	Density	Lack of data
k_m	1 [W/(mK)]	Thermal conductivity	Lack of data

Table A.3: Material parameters of LFP particles. Reference lack of data meaning that assumption has been made.

Parameter	Value [Unit]	Description	Ref.
E_p	125 [GPa]	Elastic modulus	[23]
G_p	1 [GPa]	Shear modulus	Lack of data
ν_p	0.28 [-]	Poisson's ratio	Lack of data
α_p	$1 * 10^{-6}$ [1/K]	Thermal expansion coeff.	Lack of data
$C_{p,p}$	1.5 [J/(gK)]	Specific heat capacity	Lack of data
ρ_p	3600 [kg/m^3]	Density	Lack of data
k_p	50 [W/(mK)]	Thermal conductivity	Lack of data
V_p	0.48 [-]	Volume fraction	Chosen value

Table A.4: Material parameters of polyethylene (PE). Reference COMSOL means that these values where taken from the COMSOL material library.

Parameter	Value [Unit]	Description	Ref.
E_{PE}	1 [GPa]	Elastic modulus	COMSOL
ν_{PE}	0.4 [-]	Poisson's ratio	Lack of data
ρ_{PE}	930 [kg/m^3]	Density	COMSOL
$C_{p,PE}$	1900 [J/(kgK)]	Specific heat capacity	COMSOL
k_{PE}	0.38 [W/(mK)]	Thermal conductivity	COMSOL
α_{PE}	$150 * 10^{-6}$ [1/K]	Thermal expansion coeff.	COMSOL
G_{PE}	0.75 [GPa]	Shear modulus	COMSOL
t_{PE}	12 [μm]	Thickness	[12]

Table A.5: Material parameters of aluminium. Reference COMSOL means that these values where taken from the COMSOL material library.

Parameter	Value [Unit]	Description	Ref.
E_{Al}	70 [GPa]	Elastic modulus	COMSOL
ν_{Al}	0.33 [-]	Poisson's ratio	COMSOL
ρ_{Al}	2700 [kg/m^3]	Density	COMSOL
$C_{p,Al}$	900 [J/(kgK)]	Specific heat capacity	COMSOL
k_{Al}	238 [W/(mK)]	Thermal conductivity	COMSOL
α_{Al}	$23 * 10^{-6}$ [1/K]	Thermal expansion coeff.	COMSOL
G_{Al}	25.5 [GPa]	Shear modulus	COMSOL
t_{Al}	9 [μm]	Thickness	[12]

Table A.6: Material parameters of polyethylene terephthalate (PET).

Parameter	Value [Unit]	Description	Ref.
E_{PET}	2.95 [GPa]	Elastic modulus	[19]
ν_{PET}	0.4 [-]	Poisson's ratio	[19]
ρ_{PET}	1375 [kg/m^3]	Density	[19]
$C_{p,PET}$	1195 [J/(kgK)]	Specific heat capacity	[19]
k_{PET}	0.24 [W/(mK)]	Thermal conductivity	[19]
α_{PET}	$70 * 10^{-6}$ [1/K]	Thermal expansion coeff.	[19]
G_{PET}	1.375 [GPa]	Shear modulus	[19]
t_{PET}	75 [μm]	Thickness	[12]

B

Materials in comsol

Here follows how the material properties is denoted in the global materials in the COMSOL model.

B.1 Battery cell

Thermal conductivity:

$$\boldsymbol{k} = \begin{bmatrix} k_L & 0 & 0 \\ 0 & k_T & 0 \\ 0 & 0 & k_T \end{bmatrix} \tag{B.1}$$

Thermal expansion coefficient:

$$\boldsymbol{\alpha} = \begin{bmatrix} \alpha_L & 0 & 0 \\ 0 & \alpha_T & 0 \\ 0 & 0 & \alpha_T \end{bmatrix} \tag{B.2}$$

Elastic modulus:

$$\boldsymbol{E} = \begin{bmatrix} E_L \\ E_T \\ E_T \end{bmatrix} \tag{B.3}$$

Poisson's ratio:

$$\boldsymbol{\nu} = \begin{bmatrix} \nu_{LT} \\ \nu_{LT} \\ \nu_{LT} \end{bmatrix} \tag{B.4}$$

Shear modulus:

$$\boldsymbol{G} = \begin{bmatrix} G_{LT} \\ G_{TT} \\ G_{LT} \end{bmatrix} \tag{B.5}$$

B.2 Pouch-bag

Thermal conductivity:

$$\boldsymbol{k} = \begin{bmatrix} k_x & 0 & 0 \\ 0 & k_x & 0 \\ 0 & 0 & k_z \end{bmatrix} \tag{B.6}$$

Thermal expansion coefficient:

$$\boldsymbol{\alpha} = \begin{bmatrix} \alpha_x & 0 & 0 \\ 0 & \alpha_x & 0 \\ 0 & 0 & \alpha_z \end{bmatrix} \tag{B.7}$$

Elastic modulus:

$$\boldsymbol{E} = \begin{bmatrix} E_x \\ E_x \\ E_z \end{bmatrix} \tag{B.8}$$

Poisson's ratio:

$$\boldsymbol{\nu} = \begin{bmatrix} \nu_{xy} \\ \nu_{xy} \\ \nu_{xy} \end{bmatrix} \tag{B.9}$$

Shear modulus:

$$\boldsymbol{G} = \begin{bmatrix} G_{xy} \\ G_{xz} \\ G_{xz} \end{bmatrix} \tag{B.10}$$

C
Validation

The validation of the modelled framework can be conducted in two ways: firstly the materials can be changed from orthotropic to isotropic materials and secondly the expansion for each layer of the battery cell (i.e. not the pouch-bag) can be tested separately.

By simplifying the model to use isotropic materials instead of orthotropic materials it is possible to validate the model behaviour. These materials often have all needed materials already known and also how they behave, in comparison with the composite materials in this thesis which both have been assumed and approximated using micro-mechanic models. If these material behave as they ought when applied to the layers in the model, then the model is sufficiently right regarding the boundary conditions and physics.

In COMSOL, expansion of a material can be assigned two different ways. Either by apply it directly in the heat transfer physics for each layer of the battery cell or by apply it in the multi-physics. These two ways, if the model is correct, shall give the same result. Each layer of the battery cell is then tested separately with both expansions. For this to work a heat source need to be applied and also boundary conditions. Here, the boundary conditions explained in section 3.1.3 is used. No heat source will give no expansion as there is no temperature change, i.e. the pouch-bag cannot be tested individually. If these two expansion for each layer are the same, it means that the material properties are assigned correctly to the material.

The three Figures below show the strains (expansion) for each layer separately. These strains are the same regardless which expansion technique used.

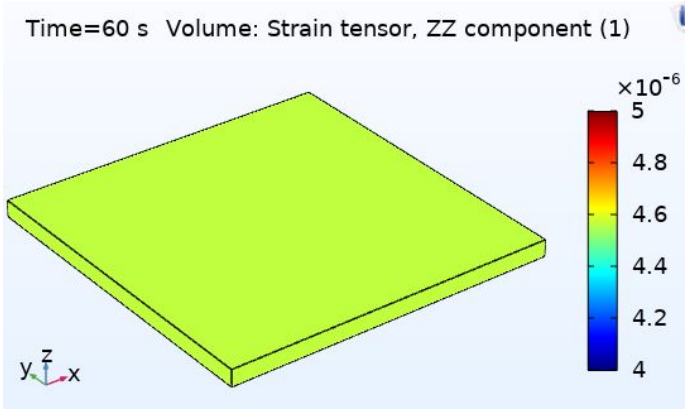

Figure C.1: Expansion induced strains, with a value of $4.56 * 10^{-6}$, in the negative electrode with a heat source of 500 kW/m^3 and heat transfer coefficient 5 W/(m^{2}K).

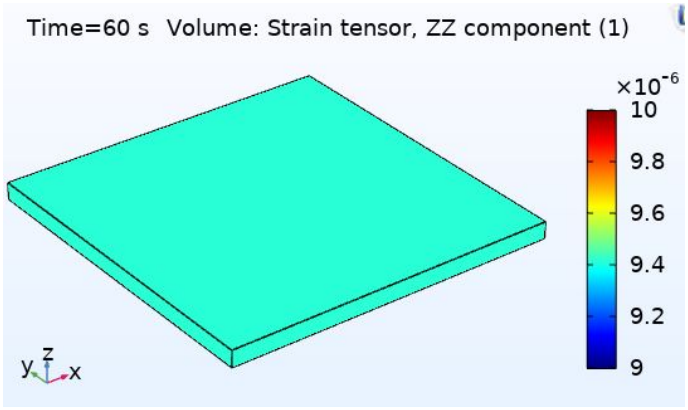

Figure C.2: Expansion induced strains, with a value of $9.42 * 10^{-6}$, in the separator with a heat source of 500 kW/m^3 and heat transfer coefficient 5 W/(m^{2}K).

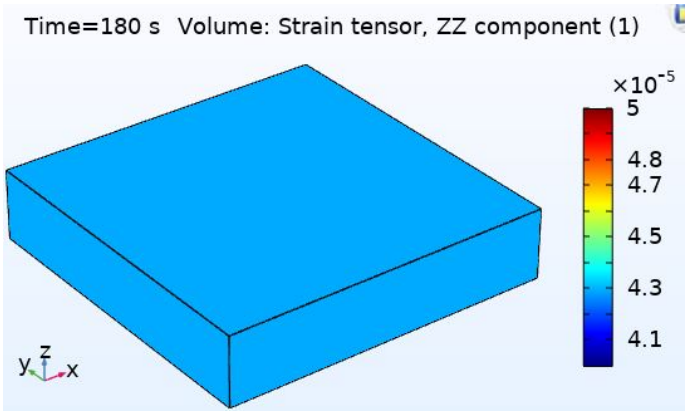

Figure C.3: Expansion induced strains, with a value of $4.29 * 10^{-5}$, in the positive electrode with a heat source of 500 kW/m^3 and heat transfer coefficient 5 W/(m^{2}K).